

**Large-eddy simulation
of turbulent flows**

Ugo Piomelli

*Department of Mechanical Engineering
University of Maryland
College Park, MD 20742*

July 22, 1994

Contents

Acknowledgments	iii
1 Introduction	1
1. Overview	1
2. Motivation	1
3. Simulation techniques	2
3.1. Reynolds-averaged Navier-Stokes equations (RANS)	2
3.2. Direct numerical simulation (DNS)	3
3.3. Large-eddy simulation (LES)	3
2 The subgrid-scale stresses.	5
1. The filtering operation	5
2. Filtered Navier-Stokes equations	7
3. The subgrid-scale stresses	8
4. Favre-filtering	8
5. Energy transfer mechanisms	9
3 Numerical methods	17
1. Spatial discretization	17
2. Time advancement	18
3. Boundary conditions	18
4. Initial conditions	20
4 Subgrid-scale models and applications	23
1. Introduction	23
2. Smagorinsky model	24
3. Two-point closures	30
4. Renormalization Group theory	32
5. Dynamic models	34
6. Scale-similar models	38
7. One-equation models	41
8. Wall layer models	43
9. Backscatter modeling	46

5	Conclusions	49
6	Bibliography	53

Acknowledgments

This report is based on a Short Course of the same title given during a sabbatical stay at the Theoretical and Applied Mechanics Department of the University of Illinois at Urbana-Champaign between January and April, 1994. I wish to thank Professors Ronald J. Adrian and Hassan Aref for having invited me; I remain indebted to them and to the other faculty and staff at TAM for the gracious and generous hospitality that was extended to me there. The financial support provided by the Air Force Office of Scientific Research under Contract Number AFOSR 90-0169, and by the Theoretical and Applied Mechanics Department is gratefully acknowledged. Professors Kyle D. Squires and Andrzej Domaradzki, Ms. Junhui Liu, and Messrs. Xiaoli Huai, Elias Balaras and Chandrasekhar Kanepalli supplied several helpful comments on the manuscript.

Chapter 1

Introduction

1. Overview

Over twenty years have passed since the first large eddy simulation (LES) results by Deardorff (1970) were published. During this period, this technique has matured considerably: the underlying theory has been advanced, new models have been developed and tested, more efficient numerical schemes have been used. The progress in computer power and memory has made possible the application of LES to a variety of flows, compressible and incompressible, including heat transfer, stratification, passive scalars and chemical reactions.

The present report is a general review of the present state of this technique. Additional analyses of various aspects of LES can be found in the review articles by Rogallo and Moin (1984), Yoshizawa (1987) and Reynolds (1990) and the book by Lesieur (1990), to which the reader is referred.

2. Motivation

Turbulence is a phenomenon that occurs frequently in nature; it has, therefore, been the subject of study for over one hundred years. In 1510, Leonardo da Vinci accompanied a drawing of the vortices shed behind a blunt obstacle with the following observation (Richter 1970):

Observe the motion of the water surface, which resembles that of hair, that has two motions: one due to the weight of the shaft, the other to the shape of the curls; thus, water has eddying motions, one part of which is due to the principal current, the other to the random and reverse motion.

Although based entirely on speculation, and not accompanied by a mathematical analysis, this observation may be seen as a precursor to Reynolds' decomposition of velocity, pressure and other variables into mean and fluctuating parts.

In present days, the prediction and control of turbulent flows has become increasingly important, due to their frequent occurrence in technological applications involving transportation systems (cars, aircraft and ships), energy conversion systems (engines, turbines, compressors) and geophysical applications (weather prediction, pollutant dispersion). The need for accurate models of turbulent flows is presently the pacing item for the development of more accurate design and

analysis tools for the applications mentioned above. For these reasons, added stress has been placed in recent years on the development of accurate numerical tools for the prediction of turbulent flows.

3. Simulation techniques

Analytical or numerical solution of turbulent flow problems can be accomplished using various levels of approximation, yielding more or less detailed descriptions of the state of the flow. The simplest approach is to use semi-empirical correlations. Moody's diagram, which gives the skin friction factor for cylindrical pipes as a function of Reynolds number and relative roughness, is an example of this approach, which is especially useful for global, control-volume analyses, but that yields no information on local quantities and relies heavily on the availability of experimental data in configurations similar to the one under study.

3.1. Reynolds-averaged Navier-Stokes equations (RANS)

A more sophisticated method involves the use of Reynolds' averaging: the long-time average of a quantity f is defined as

$$\bar{f}(t) = \frac{1}{T} \int_{t-T}^t f(\tau) d\tau, \quad (1.1)$$

where T is a time interval much longer than all the time scales of the turbulent flow. The averaging operation defined above permits one to decompose any quantity into its mean part, \bar{f} , and a fluctuating part, $f - \bar{f}$. If the averaging operation (1.1) is applied to the equations of motion, one obtains the well-known Reynolds-averaged Navier-Stokes equations, that describe the evolution of the mean quantities. The effect of turbulent fluctuations appears in a Reynolds stress term that must be modeled to close the system.

Among the most commonly used models for the Reynolds-averaged Navier-Stokes equations are mixing length models, $k - \varepsilon$ models, and full or algebraic Reynolds stress closures. A common limitations of these models is their lack of generality: the model constants are usually set using a few simple flows, for which theoretical solutions are known or well-documented experiments are available. When the models are applied to flows that are very different from the ones used for calibration, however, the constants often have to be adjusted to yield accurate predictions. Furthermore, laminar-turbulent transition is exceedingly difficult to predict using the RANS approach, and requires the addition of significant semi-empirical data, usually in the form of intermittency functions.

The principal reason for the lack of generality of turbulence models lies in the fact that the model must represent a very wide range of scales. While the small scales tend to depend only on viscosity, and may, therefore, be somewhat universal, the large ones are affected very strongly by the boundary conditions (see, for instance, the difference between the spanwise rollers present in mixing layers and wakes and the elongated streamwise vortices that are found in the near-wall region of a turbulent boundary layer). Thus, it does not seem possible to model the effect of the large scales of turbulence in the same way in flows that are very different.

3.2. Direct numerical simulation (DNS)

The most straightforward approach to the solution of turbulent flows is the direct numerical simulation (DNS) of turbulence, in which the governing equations are discretized and solved numerically. If the mesh is fine enough to resolve even the smallest scales of motion, and the scheme is designed to minimize the numerical dispersion and dissipation errors, one can obtain an accurate three-dimensional, time-dependent solution of the governing equations completely free of modeling assumptions, and in which the only errors are those introduced by the numerical approximation.

DNS has been a very useful tool, over the past ten years, for the study of transitional and turbulent flow physics, but it also has some serious limitations. First, the use of highly accurate, high-order schemes is desirable to limit dispersion and dissipation errors; these schemes (spectral methods, for example) tend to have little flexibility in handling complex geometries and general boundary conditions. Secondly, to resolve all scales of motion, one requires a number of grid points $N \sim L/\eta$, where L is the dimension of the computational domain (the largest scale in the system) and η is the smallest scale of motion, the Kolmogorov length scale. Since this ratio is proportional to $Re^{3/4}$, the number of grid points required by a DNS goes like $N^3 \sim Re^{9/4}$; furthermore, the operation count of typical CFD codes is proportional to $N^3 \log N$, and the number of timesteps required to advance the computation for a given period scales like $Re^{3/4}$. Altogether, the cost of a computation is proportional to at least Re^3 . Thus, to increase the Reynolds number by a factor of two the computational effort must increase by at least a factor of 8. For these reasons, DNS has largely been limited to simple geometries (flat plate, homogeneous flows) at low Reynolds numbers, and its application to engineering-type problems within the next decade appears unlikely.

3.3. Large-eddy simulation (LES)

Large-eddy simulation (LES) is a technique intermediate between the direct simulation of turbulent flows and the solution of the Reynolds-averaged equations. In LES the contribution of the large, energy-carrying structures to momentum and energy transfer is computed exactly, and only the effect of the smallest scales of turbulence is modeled. Since the small scales tend to be more homogeneous and universal, and less affected by the boundary conditions than the large ones, there is hope that their models can be simpler and require fewer adjustments when applied to different flows than similar models for the RANS equations.

LES is similar to DNS in that it provides a three-dimensional, time dependent solution of the Navier-Stokes equations. Thus, it still requires fairly fine meshes. However, it can be used at much higher Reynolds numbers than DNS; ideally, in fact, if the small scales obey inertial range dynamics, the cost of a computation is independent of Re (not, however, if a solid boundary is present).

LES is a promising technique for the calculation of turbulent flows of engineering interest. In the following chapters various aspects of its implementation will be discussed and some applications of LES to engineering flows, mostly incompressible, will be presented. Chapter 2 will discuss the subgrid-scale stresses and the energy exchange mechanisms that must be reproduced by SGS

models; Chapter 3 will concentrate on numerical issues; in Chapter 4 various SGS models will be discussed. Finally, in Chapter 5, final considerations will be made.

Chapter 2

The subgrid-scale stresses.

1. The filtering operation

To separate the large from the small scales, LES is based on the definition of a filtering operation: a filtered (or resolved, or large-scale) variable, denoted by an overbar, is defined as

$$\bar{f}(\mathbf{x}) = \int_D f(\mathbf{x}') G(\mathbf{x}, \mathbf{x}') d\mathbf{x}', \quad (2.1)$$

where D is the entire domain and G is the *filter* function. The filter function determines the size and structure of the small scales. It is easy to show that, if G is a function of $\mathbf{x} - \mathbf{x}'$ only, differentiation and the filtering operation commute (Leonard 1974).

The most commonly-used filter functions are the sharp Fourier cutoff filter, best defined in wave space¹ as

$$\hat{G}(k) = \begin{cases} 1 & \text{if } k \leq \pi/\Delta \\ 0 & \text{otherwise,} \end{cases} \quad (2.2)$$

the Gaussian filter,

$$G(x) = \sqrt{\frac{6}{\pi\Delta^2}} \exp\left(-\frac{6x^2}{\Delta^2}\right), \quad (2.3)$$

and the tophat filter in real space:

$$G(x) = \begin{cases} 1/\Delta & \text{if } |x| \leq \Delta/2 \\ 0 & \text{otherwise,} \end{cases} \quad (2.4)$$

these three filters and their Fourier transforms are shown in Figure 2.1. It should be noticed that the Gaussian filter is used in conjunction with a sharp Fourier cutoff. The truncation of the Gaussian at a non-negligible value is the cause for the ringing observed in the figure. For uniform filter width Δ^2 the filters above are mean-preserving and commute with differentiation.

To illustrate the difference between the filters defined above they are applied, in Figure 2.2, to a test function with a realistic spectrum. The Fourier cutoff filter is seen to reproduce better the smallest resolved scales of motion. Tophat and Gaussian filters give similar results, as also shown

¹Unless otherwise noted, quantities denoted by a caret $\hat{\cdot}$ are the complex Fourier coefficients of the original quantity.

²For a discussion of filtering with non-uniform filters see Ghosal (1994).

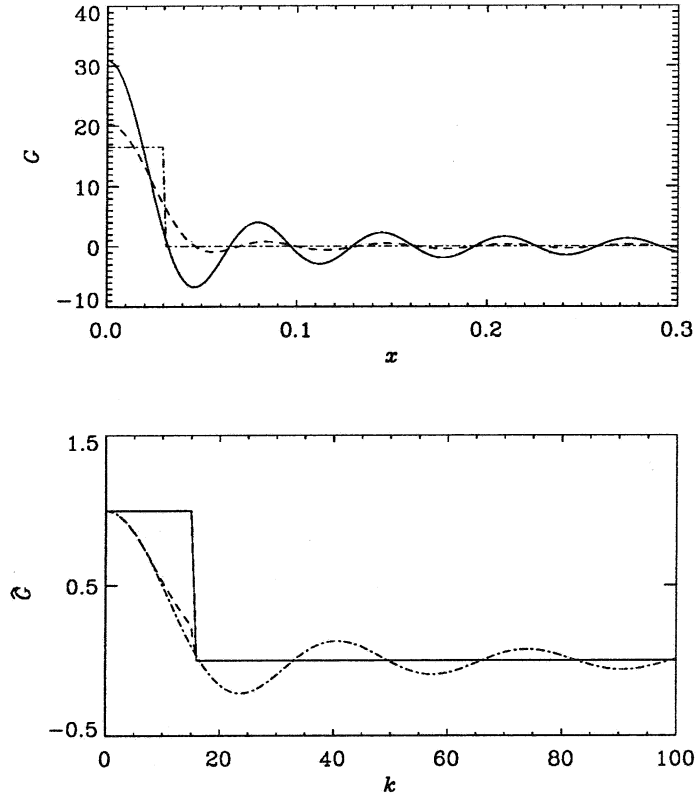


Figure 2.1: Typical filter functions. — : sharp Fourier cutoff; --- : truncated Gaussian; —·— : tophat. Top: real space; bottom: Fourier transform.

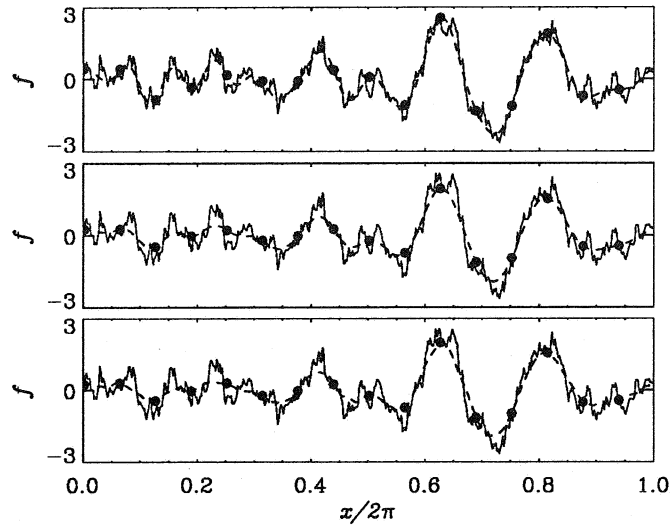


Figure 2.2: Filtering of a test function. — : Unfiltered; --- : filtered. Top: sharp Fourier cutoff; middle: Gaussian; bottom: tophat. The dots represent the value of the filtered function on a discrete mesh.

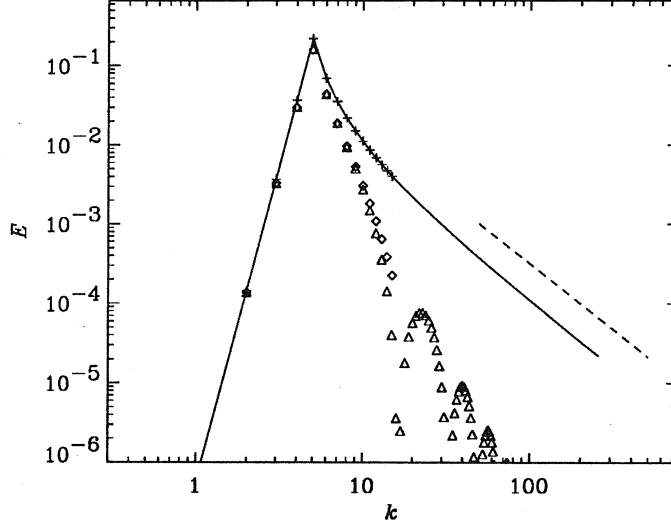


Figure 2.3: Filtering of a test function. — : Unfiltered; --- $k^{-5/3}$; + : sharp Fourier cutoff; ◇ : Gaussian; △ : tophat.

by the spectra of the filtered variables, shown in Figure 2.3. In particular, they both smooth the large-scale fluctuations as well as the small-scale ones, unlike the Fourier cutoff, that only affects the scales below the cutoff wavenumber.

2. Filtered Navier-Stokes equations

If the filtering operation (2.1) is applied to the governing equations, one obtains the filtered equations of motion. For an incompressible flow of a Newtonian fluid, they take the following form:

$$\frac{\partial \bar{u}_i}{\partial x_i} = 0. \quad (2.5)$$

$$\frac{\partial \bar{u}_i}{\partial t} + \frac{\partial}{\partial x_j} (\bar{u}_i \bar{u}_j) = -\frac{1}{\rho} \frac{\partial \bar{p}}{\partial x_i} - \frac{\partial \tau_{ij}}{\partial x_j} + \nu \frac{\partial^2 \bar{u}_i}{\partial x_j \partial x_j}. \quad (2.6)$$

$$(2.7)$$

The filtered Navier-Stokes equations, written above, govern the evolution of the large, energy-carrying, scales of motion. The effect of the small scales appears through a subgrid-scale (SGS) stress term,

$$\tau_{ij} = \overline{u_i u_j} - \bar{u}_i \bar{u}_j, \quad (2.8)$$

that must be modeled.

3. The subgrid-scale stresses

If the subgrid scale velocity $u'_i = u_i - \bar{u}_i$ is defined, the SGS stresses can be decomposed into three parts (Leonard 1974):

$$\tau_{ij} = \overline{u_i u_j} - \bar{u}_i \bar{u}_j = L_{ij} + C_{ij} + R_{ij}, \quad (2.9)$$

where $L_{ij} = \overline{u_i u_j} - \bar{u}_i \bar{u}_j$ are the Leonard stresses, $C_{ij} = \overline{u_i u'_j} + \overline{u'_j u_i}$ are the cross terms, and $R_{ij} = \overline{u'_i u'_j}$ are the SGS Reynolds stresses. The Leonard stresses represent interactions between resolved scales that result in subgrid-scale contributions. They can be computed explicitly, and, when the sharp cutoff filter is used they are the aliasing errors. The cross terms represent interactions between resolved and unresolved scales, whereas the SGS Reynolds stresses represent interactions between small, unresolved, scales. While the SGS stresses are invariant with respect to a Galilean transformation, neither L_{ij} nor C_{ij} are (Speziale, 1985). For this and other reasons (see Germano, 1986), the decomposition (2.9) has largely been abandoned.

4. Favre-filtering

In compressible flows, it is convenient to use Favre-filtering (Favre 1965a, 1965b) to avoid the introduction of subgrid-scale terms in the equation of conservation of mass. A Favre-filtered variable is defined as:

$$\tilde{f} = \frac{\overline{\rho f}}{\bar{\rho}}; \quad (2.10)$$

the Favre-filtered equations of motion then can be written in the form:

$$\frac{\partial \bar{\rho}}{\partial t} + \frac{\partial}{\partial x_j} (\bar{\rho} \tilde{u}_j) = 0, \quad (2.11)$$

$$\frac{\partial}{\partial t} (\bar{\rho} \tilde{u}_i) + \frac{\partial}{\partial x_j} (\bar{\rho} \tilde{u}_i \tilde{u}_j) = -\frac{\partial \bar{p}}{\partial x_i} - \frac{\partial \tau_{ij}}{\partial x_j} + \frac{\partial \tilde{\sigma}_{ij}}{\partial x_j}, \quad (2.12)$$

$$C_v \left[\frac{\partial}{\partial t} (\bar{\rho} \tilde{T}) + \frac{\partial}{\partial x_j} (\bar{\rho} \tilde{u}_j \tilde{T}) \right] = -\bar{p} \frac{\partial \tilde{u}_j}{\partial x_j} + \tilde{\sigma}_{ij} \frac{\partial \tilde{u}_j}{\partial x_i} + \frac{\partial}{\partial x_j} \left(\tilde{\kappa} \frac{\partial \tilde{T}}{\partial x_j} \right) - C_v \frac{\partial Q_j}{\partial x_j}. \quad (2.13)$$

The thermal energy equation is commonly used instead of the total energy conservation equation to minimize the number of SGS correlation terms that require closure. The SGS stresses and heat fluxes that must be modeled in the Favre-filtering approach are:

$$\sigma_{ij} = -\frac{2}{3} \delta_{ij} \mu \frac{\partial u_k}{\partial x_k} + \mu \left(\frac{\partial u_i}{\partial x_j} + \frac{\partial u_j}{\partial x_i} \right), \quad (2.14)$$

$$\tau_{ij} = \bar{\rho} (\widetilde{u_i u_j} - \tilde{u}_i \tilde{u}_j), \quad (2.15)$$

$$Q_k = \bar{\rho} (\widetilde{u_k T} - \tilde{u}_k \tilde{T}). \quad (2.16)$$

5. Energy transfer mechanisms

It is useful, in order to develop SGS models, to understand the physical phenomena that the models should represent. Arguably, the most important effect of the subgrid scales on the large ones, and the one that the model must represent accurately, is the energy exchange that results from the interaction between resolved and unresolved scales. To understand this interaction better, consider the transport equations for $\bar{q}^2 = \bar{u}_i \bar{u}_i$, twice the total resolved energy (mean and fluctuating), and $q_{sgs}^2 = \tau_{kk}$, twice the subgrid-scale kinetic energy:

$$\begin{aligned} \frac{\partial \bar{q}^2}{\partial t} + \underbrace{\frac{\partial}{\partial x_j} (\bar{q}^2 \bar{u}_j)}_{\text{I}} = & \underbrace{-2 \frac{\partial}{\partial x_j} (\bar{p} \bar{u}_j)}_{\text{II}} + \underbrace{\frac{\partial}{\partial x_j} \left(\nu \frac{\partial \bar{q}^2}{\partial x_j} \right)}_{\text{III}} \\ & \underbrace{-2 \frac{\partial}{\partial x_j} (\tau_{ij} \bar{u}_i)}_{\text{IV}} - \underbrace{2 \nu \frac{\partial \bar{u}_i}{\partial x_j} \frac{\partial \bar{u}_i}{\partial x_j}}_{\text{V}} + \underbrace{2 \tau_{ij} \bar{S}_{ij}}_{\text{VI}} \end{aligned} \quad (2.17)$$

$$\begin{aligned} \frac{\partial q_{sgs}^2}{\partial t} + \underbrace{\frac{\partial}{\partial x_j} (q_{sgs}^2 \bar{u}_j)}_{\text{VII}} = & \underbrace{-\frac{\partial}{\partial x_j} (\bar{u}_i \bar{u}_i \bar{u}_j - \bar{q}^2 \bar{u}_j)}_{\text{VIII}} - \underbrace{2 \frac{\partial}{\partial x_j} (\bar{p} \bar{u}_j - \bar{p} \bar{u}_j)}_{\text{IX}} + \underbrace{\frac{\partial}{\partial x_j} \left(\nu \frac{\partial q_{sgs}^2}{\partial x_j} \right)}_{\text{X}} \\ & \underbrace{+ 2 \frac{\partial}{\partial x_j} (\tau_{ij} \bar{u}_i)}_{\text{XI}} - \underbrace{2 \nu \left(\frac{\partial \bar{u}_i}{\partial x_j} \frac{\partial \bar{u}_i}{\partial x_j} - \frac{\partial \bar{u}_i}{\partial x_j} \frac{\partial \bar{u}_i}{\partial x_j} \right)}_{\text{XII}} - \underbrace{2 \tau_{ij} \bar{S}_{ij}}_{\text{XIII}}. \end{aligned} \quad (2.18)$$

The equations above show that the resolved scales in a control volume (a grid cell, for example), exchange energy with the unresolved scales and the surroundings through the following mechanisms:

- I Advection.
- II Diffusion by pressure forces.
- III Viscous diffusion.
- IV Diffusion due to the subgrid scale stresses.
- V Viscous dissipation.
- VI Subgrid-scale dissipation.

The first four terms do not create or destroy resolved energy but only redistribute it between adjoining volumes. Term V represents the resolved energy lost by viscous dissipation at the resolved scale level, while the last one, the subgrid-scale dissipation $\varepsilon_{sgs} = \tau_{ij} \bar{S}_{ij}$, represents the net energy exchange between the resolved and unresolved scales, and can be positive or negative. On the average, energy flows from the large to the small scales, and $\varepsilon_{sgs} < 0$ (forward scatter); backscatter occurs when the energy flow is reversed ($\varepsilon_{sgs} > 0$). The total transfer of energy between large and subgrid scales is the SGS transport, sum of terms IV and VI.

The energy exchange mechanisms for the subgrid scales are similar:

VII Advection.

VIII Turbulent transport.

IX Diffusion by pressure forces.

X Viscous diffusion.

XI Diffusion due to the subgrid scale stresses.

XII Viscous dissipation.

XIII Subgrid-scale dissipation.

Terms VII through X are again redistribution terms. The energy lost by the resolved scales to the subgrid ones appears as a source term in the transport equation for q_{sgs}^2 : terms XI and XIII have opposite signs in (2.17) and (2.18). It is important to point out the difference between terms XII and XIII. The former is the SGS dissipation ε_{sgs} , that represents an energy interchange between resolved and unresolved scales, and is generally a dissipative term in the equation for \bar{q}^2 , a production term in the equation for q_{sgs}^2 . Term XII, on the other hand, represents the SGS energy dissipated by the viscous forces.

Equations for the average energies can be obtained by defining an ensemble average $\langle \cdot \rangle$ such that $F = \langle \bar{f} \rangle$ (where $F = \langle f \rangle$). Let $\bar{f}'' = \bar{f} - F$ and $f'' = f - F$ represent resolved or total fluctuating quantities, and define the operator

$$\frac{D_U}{Dt} = \frac{\partial}{\partial t} + U_j \frac{\partial}{\partial x_j}. \quad (2.19)$$

The transport equations for $\langle u_i'' u_i'' \rangle$ (twice the total turbulent kinetic energy), $\langle \bar{u}_i'' \bar{u}_i'' \rangle$ (twice the resolved turbulent kinetic energy), and $\langle \tau_{ii} \rangle = \langle q_{sgs}^2 \rangle$ are of the form

$$\frac{D_U}{Dt} \langle u_i'' u_i'' \rangle = \underbrace{-2 \langle u_i'' u_j'' \rangle \frac{\partial U_i}{\partial x_j}}_A - \underbrace{\frac{\partial}{\partial x_j} \langle u_i'' u_i'' u_j'' \rangle}_{B} + \dots \quad (2.20)$$

$$\begin{aligned} \frac{D_U}{Dt} \langle \bar{u}_i'' \bar{u}_i'' \rangle = & \underbrace{-2 \langle \bar{u}_i'' \bar{u}_j'' \rangle \frac{\partial U_i}{\partial x_j}}_C - \underbrace{2 \langle \tau_{ij} \rangle \frac{\partial U_i}{\partial x_j}}_D - \underbrace{\frac{\partial}{\partial x_j} \langle \bar{u}_i'' \bar{u}_i'' \bar{u}_j'' \rangle}_E \\ & \underbrace{-2 \frac{\partial}{\partial x_j} \langle \tau_{ij} \bar{u}_i \rangle}_F + \underbrace{2 \langle \tau_{ij} \bar{S}_{ij} \rangle}_G + \dots \end{aligned} \quad (2.21)$$

$$\begin{aligned} \frac{D_U}{Dt} \langle \tau_{ii} \rangle = & \underbrace{-\frac{\partial}{\partial x_j} \langle u_i'' u_i'' u_j'' - \bar{u}_i'' \bar{u}_i'' \bar{u}_j'' \rangle}_H \\ & \underbrace{+2 \frac{\partial}{\partial x_j} \langle \tau_{ij} \bar{u}_i \rangle}_I - \underbrace{2 \langle \tau_{ij} \bar{S}_{ij} \rangle}_J + \dots \end{aligned} \quad (2.22)$$

The production term in the equation for $\langle u_i'' u_i'' \rangle$ (term A) generates two terms in the equation for $\langle \bar{u}_i'' \bar{u}_i'' \rangle$, C and D. Term C represents the production of resolved energy by interactions between resolved scales, while D represents the production of resolved energy by interactions between the mean velocity gradient and SGS stresses. The turbulent diffusion term, B, also gives rise to two terms; one of them, E, represents the change of resolved energy due to the turbulent diffusion of the resolved scales; the second, H, represents the change in SGS energy due to the turbulent diffusion of resolved and unresolved scales. The terms F+G, and their counterparts in the SGS equation, I+J, represent energy exchanges between the resolved and unresolved scales.

One way to study SGS physics and evaluate SGS models is the *a priori* test, in which a velocity field u_i obtained from a well-resolved “experiment” (either a DNS, or PIV or hot-wire measurements) is subjected to the filtering operation to yield \bar{u}_i ; u_i and \bar{u}_i can then be used to calculate the desired SGS quantities, and compare them to the predictions of a model.

Piomelli *et al.* (1991) used the *a priori* test to study the subgrid-scale energy transfer in plane channel flow and isotropic turbulence. They found that backward and forward scatter are almost equal in magnitude, and each is much larger than the SGS dissipation. The magnitude of SGS dissipation and SGS backscatter increases with filter width, and backscatter occurs at nearly 50% of the points. Furthermore, regions of coherent forward and backward energy transfer appeared to be strongly correlated with regions where large resolved stress $\bar{u}'' \bar{v}''$ was also observed.

Several mathematical theories of turbulence have been applied to the study of the energy transfer to a wavenumber shell k from all wavenumbers \mathbf{p} and \mathbf{q} such that $\mathbf{p} + \mathbf{q} = \mathbf{k}$. Define

$$N_i = -\frac{\partial}{\partial x_j} (u_i u_j) \quad \text{and} \quad T(\mathbf{k}) = \mathcal{R} [\hat{u}_i^* \hat{N}_i], \quad (2.23)$$

where $\mathcal{R}(z)$ denotes the real part of a complex quantity z , and z^* is the complex conjugate of z . By integrating $T(\mathbf{k})$ over all wavenumbers \mathbf{p} and \mathbf{q} such that $|\mathbf{p} + \mathbf{q}| = |\mathbf{k}|$, the energy transfer function $T(k)$ is obtained; this function is often represented in terms of an eddy viscosity

$$\nu_e(k) = -\frac{T(k)}{2k^2 E(k)}, \quad (2.24)$$

where $E(k)$ is the resolved-scale spectrum. Kraichnan (1976) used the test-field model (TFM) to study the energy transfer to wavenumbers $k < K_c$ due to interactions with unresolved scales. For a cutoff in the inertial range of the spectrum, the theory predicts that ν_e is nearly constant for $k \ll K_c$, and rises to a cusp as $k \rightarrow K_c$ (Figure 2.4). The constant eddy viscosity for small wavenumbers is due to interactions between wavenumbers $p \simeq q \gg k$; the separation of scales results in mechanisms analogous to those responsible for the molecular viscosity. For $k \simeq K_c$, however, the nonlocal interactions involving triads with either p or $q \ll K_c$ (i.e., interactions between two wavenumbers \mathbf{p} and \mathbf{q} of very different magnitude that transfer energy to a wavenumber with magnitude nearly equal to the high wavenumber mode, such as the triad $k \simeq p$, and $k, p \gg q = p - k$) dominate the energy exchange across the boundary K_c , and result in the finite cusp sketched in Figure 2.4.

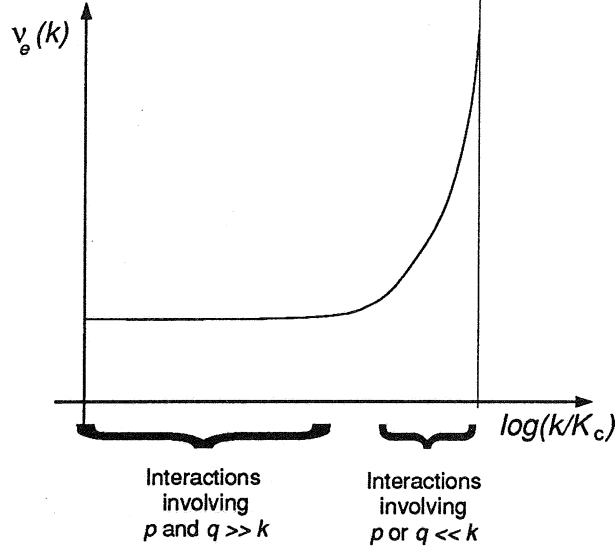


Figure 2.4: Subgrid-scale eddy viscosity in wave space.

The analysis above assumes an inertial spectrum extending from $k = 0$ to ∞ . If the spectrum is cut off at some bottom wavenumber, a rounding-off of the cusp will result; if, on the other hand, the cutoff is in an exponentially-decaying region of the spectrum (i.e., in the dissipation region), the level of the constant eddy-viscosity region will decrease, as distant interactions become less important. The cusp, however, invariably provides the greatest part of the energy transfer to the unresolved scales: numerical integration of the energy transfer function obtained by the TFM theory shows that roughly 75% of the energy transfer is due to the octave of wavenumbers $K_c/2 < k < K_c$ (Kraichnan 1976).

Domaradzki *et al.* (1993) used a DNS of homogeneous isotropic turbulence to compute $\nu_e(k)$, and found that forward and backward energy transfer are both important. Figure 2.5a shows that, near the cutoff, the negative part of ν_e (corresponding to backscatter) reduces the cusp significantly; at low wavenumbers, moreover, backscatter is larger than the forward scatter. The cusp-like behavior of the eddy viscosity predicted by the theory was observed, but no constant eddy-viscosity region is present, probably due to the low Reynolds number of the DNS, which causes the cutoff K_c to be in the dissipative region of the spectrum. In Figure 2.5b the contribution of the unresolved scales closest to the cutoff to ν_e is shown. Most of the SGS energy transfer appears to be due to the octave below the cutoff, that is to wavenumbers $K_c < k < 2K_c$. The observation that SGS energy transfer is due to highly-correlated modes near the cutoff implies that stochastic models of the reverse energy transfer may not be appropriate. Furthermore, the work of Domaradzki *et al.* (1993) confirms the theoretical finding that the predominant mechanism is a local energy transfer due to nonlocal interactions.³

³Interactions involving at least two scales with wavenumber ratio greater than two are defined by Domaradzki *et al.* (1993) as “nonlocal”. Using a larger ratio is unfeasible because of the limited range of scales present in the DNS data.

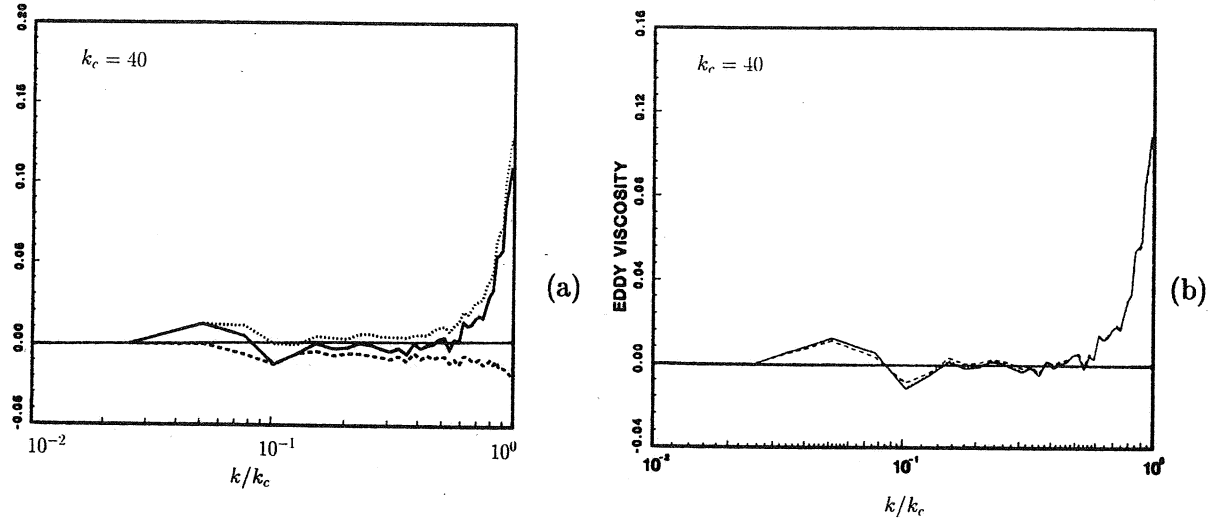


Figure 2.5: Subgrid-scale eddy viscosity in wave space. Homogeneous isotropic turbulence (from Domaradzki *et al.* 1993). (a) — Total; positive part; --- negative part. (b) — Total; --- contribution of modes $K_c < k < 3K_c/2$; contribution of modes $K_c < k < 2K_c$.

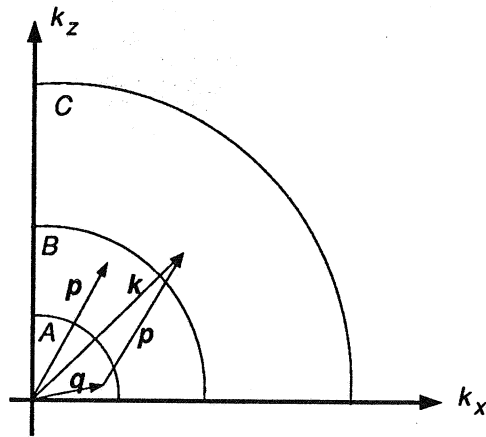


Figure 2.6: Energy transfer integrated over wavenumber bands.

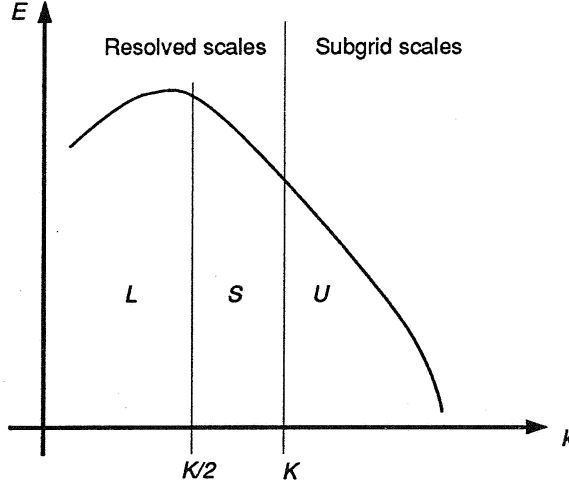


Figure 2.7: Wavenumber bands for the integrated energy transfer.

An extension of the previous study was carried out by Domaradzki *et al.* (1994). To quantify better the effect of local and nonlocal interactions on the energy transfer to the unresolved scales, they divided the wavenumber space into three bands, and integrated $T(\mathbf{k})$ over all wavenumbers triads $\mathbf{p}, \mathbf{q}, \mathbf{k}$ such that $\mathbf{p} \in B$, $\mathbf{q} \in A$, and $\mathbf{k} = \mathbf{p} + \mathbf{q} \in C$ (Figure 2.6). The energy transfer function obtained in this fashion was denoted by T^{ABC} . The k_x, k_z space (Figure 2.7) was subdivided into a region L containing the large resolved scales, a region S containing the smallest resolved scales, and one, U , including the unresolved scales. The energy transferred between bands was then computed from a DNS of plane channel flow as a function of the distance from the wall. Their results indicate that the transfer to the small resolved scales S accounts for nearly all the SGS energy transfer. Furthermore (Figure 2.8), they show that nonlocal transfer directly from the largest to the smallest scales of motion (T^{LUU} in the convention defined above) is not very significant.

In conclusion, an accurate SGS model should be able to predict correctly the energy exchange between resolved and unresolved scales. While, on average, the subgrid scales drain energy from the resolved ones, backward and forward scatter have been shown to be very significant. The principal interactions, moreover, have been shown to take place between the octave above the cutoff ($K_c/2 < k < K_c$) and the octave below it ($K_c < k < 2K_c$). In Chapter 4, several models and their applications, will be discussed.

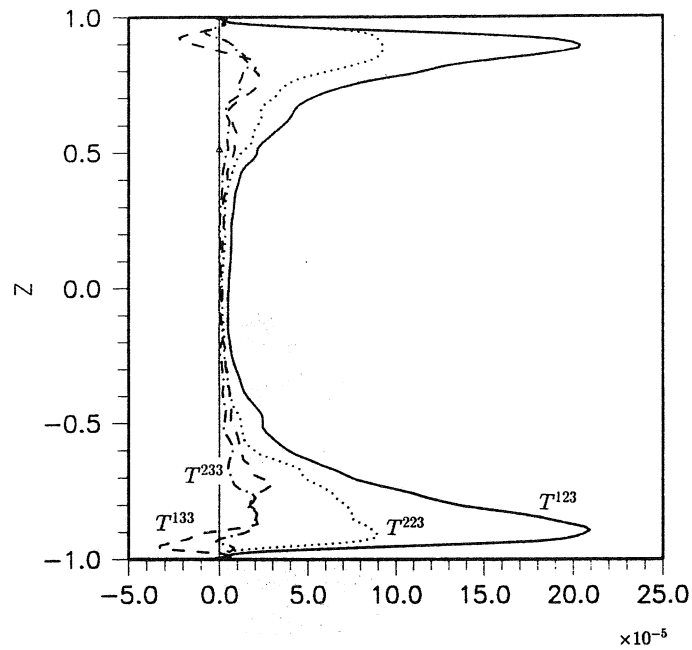


Figure 2.8: Total transfer to the subgrid scales (LSU+LUU+SSU+SUU) (from Domaradzki *et al.* 1994). The wall-normal coordinate is z . — LSU; --- LUU; SSU; — SUU.

Chapter 3

Numerical methods

1. Spatial discretization

The analytical derivative of a complex exponential $f(x) = e^{ikx}$ is $f'(x) = ik e^{ikx}$; if f is differentiated numerically, however, the result is

$$\frac{\delta f}{\delta x} = ik' e^{ikx}, \quad (3.1)$$

where k' is the modified wavenumber. A modified wavenumber corresponds to each differencing scheme; the real part of k' represents the attenuation of the computed derivative compared to the actual one, whereas a non-zero imaginary part of k' indicates that phase errors are introduced by the numerical differentiation. For a second-order centered scheme, for instance, $k' = k \sin k\Delta x / k\Delta x$. For small wavenumbers k the numerical derivative is quite accurate; high wavenumber fluctuations, however, are resolved increasingly poorly. No phase errors are introduced. Figure 3.1 shows a sketch of the real part of the modified wavenumbers for various numerical schemes.

The need to resolve accurately high wavenumber turbulent fluctuations implies that either low-order schemes must be used on very fine meshes, or that higher-order schemes are required on coarser meshes. High-order schemes are more expensive, in terms of computational resources, than low-order ones, but the increase in accuracy they afford, for a given mesh, often justifies their use.

Most LES (and DNS) calculations, to date, have been performed using spectral schemes (Fourier expansions in homogeneous directions, Chebychev polynomials in inhomogeneous ones, for instance). These methods are very accurate, but tend to be more expensive than finite-difference schemes, and also give little flexibility in the application of the boundary conditions.

Finite difference schemes, second-order or higher, are also used, although less frequently. As the application of LES shifts from basic, building-block flows in simple geometries towards more realistic applications, however, the additional flexibility that finite differences enjoy in the treatment of complex geometries and boundary conditions is resulting in more widespread application of these methods.

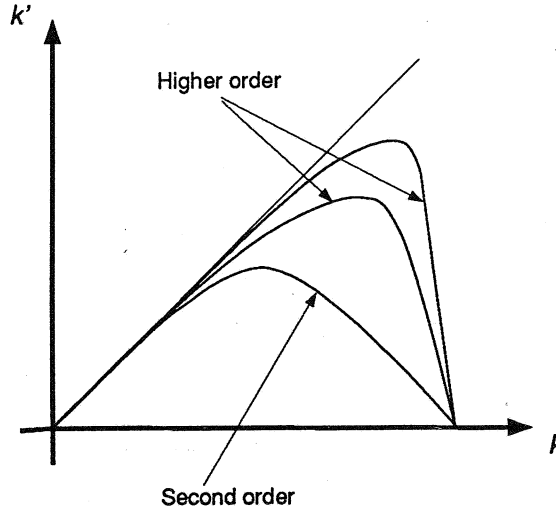


Figure 3.1: Modified wavenumber for various numerical schemes.

2. Time advancement

The choice of time advancement method is usually determined by the requirements that numerical stability be assured and that the turbulent motions be accurately resolved in time. Two stability limits apply to LES calculations. The first is the viscous condition, that requires that the timestep Δt be less than $\Delta t_v = \sigma \Delta y^2 / \nu$ (where σ depends on the actual time advancement chosen; for implicit schemes, $\sigma = \infty$). The CFL condition requires that Δt be less than $\Delta t_c = \text{CFL} \Delta x / u$, where the maximum allowable Courant number CFL also depends on the numerical scheme used. Finally, the physical constraint requires Δt to be less than the time scale of the smallest resolved scale of motion, $\tau \sim \Delta x / U_c$ (where U_c is a convective velocity).

In most flows, the viscous condition demands a much smaller timestep than the other two; for this reason, the diffusive terms of the governing equations are usually advanced using implicit schemes (typically, the second-order Crank-Nicolson scheme). Since, however, $\Delta t_c \simeq \tau$ (usually, they differ by a factor of 3 to 6), the convective term can be advanced by explicit schemes such as the second-order Adams-Bashforth method, or third- or fourth-order Runge-Kutta schemes. In compressible flow calculations, or in unbounded flows in which the mesh must not be very fine near a solid surface, fully explicit schemes are often employed.

3. Boundary conditions

Associated with the widespread use of Fourier methods in LES is the adoption of periodic boundary conditions. Periodic boundary conditions imply that the computational domain repeats itself an infinite number of times, or that the flow is fully developed and statistically steady in space. Periodic boundary conditions are convenient, since they eliminate the need to specify inflow conditions, easy to implement (in fact they are applied implicitly by Fourier methods) and efficient, since they allow use of small computational domains.

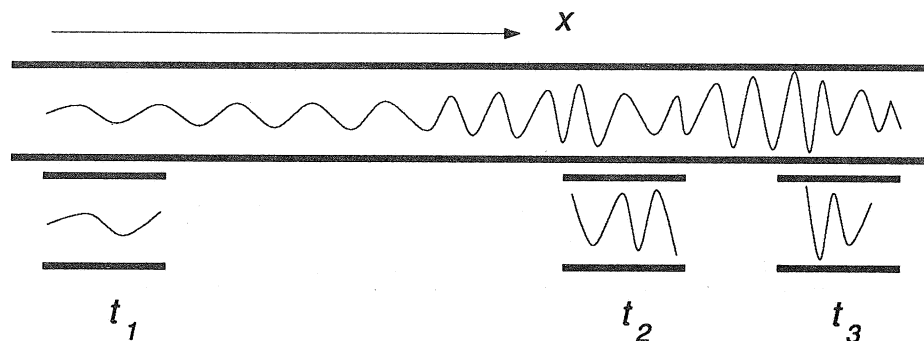


Figure 3.2: Evolution of perturbations in a channel: spatial *vs.* temporal development.

The use of periodic boundary conditions is similar to studying the time development, rather than the spatial development, of a flow; if one looks at the spatial evolution of a perturbation in plane channel (Figure 3.2), for instance, the use of periodic boundary conditions is equivalent to studying the flow in a convecting frame of reference. Each flow realization (*i.e.*, each timestep) is then equivalent to one location in the spatially-developing framework. When periodic boundary conditions are used, the computational domain must be at least as long as the wavelength of the longest structure present in the flow. If such wavelength is not known *a priori*, the two-point correlations must be examined to determine whether the domain length is sufficient.

If the flow is spatially developing, two approaches are possible: the first is the “fringe method” (Spalart and Watmuff, 1993), in which sink terms are added to the governing equations in a buffer region at the end of the domain. The purpose of these additional terms is to decrease the boundary layer thickness and, if necessary, to accelerate the decay of particular fluctuating components. These terms are active only in a small region (usually, about one quarter of the length of the computational domain), and the Navier-Stokes equations are solved everywhere else.

The specification of inflow conditions is straightforward for transitional flows, not so for turbulent flows. In all cases an entire plane of data (all velocity components) must be assigned at each instant. In transitional flows it is sufficient to specify the mean flow and the desired perturbations. For fully-developed turbulent flows one can use the same technique, but the length required for the disturbance to develop and for the flow to reach the desired turbulent state may be very significant, even if large-amplitude perturbations or random noise are given at the inflow. Alternately, one can superpose a turbulent mean flow and random noise with assigned second (or higher) moments. This approach is more physical, and requires shortened adjustment lengths, but semi-empirical information is needed to specify the inflow profiles desired. Finally, one can use the results of a periodic simulation as inflow for a non-periodic one. For instance, one can compute a turbulent channel flow and store, at each timestep, one plane, which is then used as inflow condition for the calculation of a backward facing step.

Outflow boundary conditions are usually implemented through a buffer region in which the equations are parabolized (see, for example, Street and Macaraeg, 1989). The use of the fringe method, of course, obviates the need for outflow conditions as well.

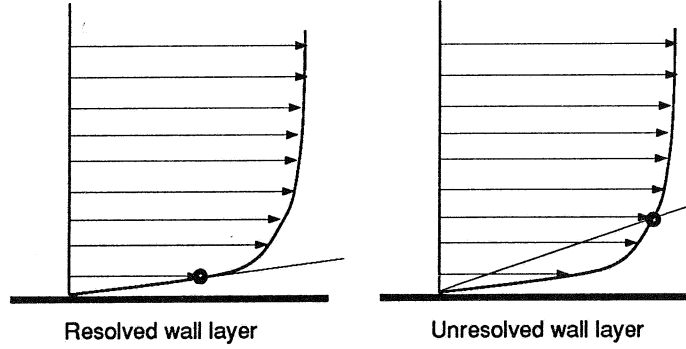


Figure 3.3: Stress at the wall.

At solid walls, the momentum flux must be known. Since the wall velocity is assigned, the no-slip condition allows the determination of the convective part $u_i u_j$ of the momentum flux at the wall. Differentiation of the velocity profile to determine the viscous part is accurate only if the wall-layer is well-resolved. To represent accurately the structures in the near-wall region, the first grid point must be located at $y^+ < 2$, Figure 3.3, and the grid spacing must be of order $\Delta x^+ \simeq 50 - 150$, $\Delta z^+ \simeq 15 - 40$. As $Re \rightarrow \infty$, an increasing number of grid points must be used to resolve a layer of decreasing thickness. Furthermore, this may result in high aspect-ratio cells, with subsequent degradation of the numerical accuracy.

When the grid is not fine enough to resolve the near-wall gradients, the momentum flux through the wall cannot be evaluated directly by numerical differentiation; the wall layer must then be modeled by specifying a correlation between the velocity in the outer flow and the stress at the wall. This approach allows the first grid point to be located at $y^+ \simeq 30 - 150$, and, since the energy-producing vortical structures in the wall-layer do not have to be resolved, it permits the use of coarser meshes in the other directions as well: $\Delta x^+ \simeq 100 - 600$, $\Delta z^+ \simeq 100 - 300$. Modeling of the wall-layer physics is, however, required, and this introduces further empiricisms in the calculations

4. Initial conditions

For flows that are statistically steady, the initial conditions are relatively unimportant. Usually, they may consist of large-amplitude perturbations superposed on a realistic mean flow, or of a fully-developed flow in a similar configuration. Typically, the flow is allowed to develop in time until a steady state is reached, and then statistics are accumulated (Figure 3.4).

For flows in which the transient is important (temporal transition, for instance, or the decay of homogeneous isotropic turbulence), more care should be used when assigning the initial conditions. In problems involving laminar-turbulent transition, controlled or random perturbations can be used. For turbulent flow problems, on the other hand, assigning random noise with a given spectrum requires some adjustment time before the nonlinear interactions become realistic.

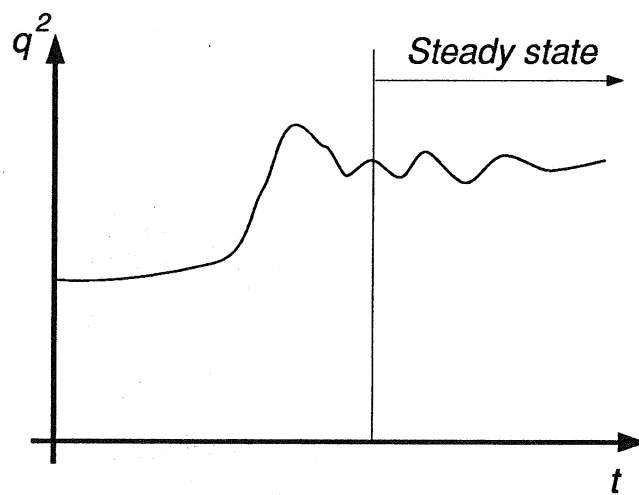


Figure 3.4: Time history in a typical time-developing calculation.

Chapter 4

Subgrid-scale models and applications

1. Introduction

Most subgrid scale models in use presently are eddy-viscosity models of the form

$$\tau_{ij} - \frac{\delta_{ij}}{3}\tau_{kk} = -2\nu_T \bar{S}_{ij}, \quad (4.1)$$

that relate the subgrid-scale stresses τ_{ij} to the large-scale strain-rate tensor

$$\bar{S}_{ij} = \frac{1}{2} \left(\frac{\partial \bar{u}_i}{\partial x_j} + \frac{\partial \bar{u}_j}{\partial x_i} \right). \quad (4.2)$$

In most cases, the eddy viscosity ν_T is obtained algebraically to avoid solving additional equations that could increase the cost of an already expensive calculation. Moreover, since the small scales tend to be more homogeneous and isotropic than the large ones, it is hoped that even simple, algebraic models can describe their physics accurately. Finally, since the SGS stresses only account for a fraction of the total stresses, modeling errors should not affect the overall accuracy of the results as much as in the standard turbulence modeling approach.

The eddy viscosity is, by dimensional analysis, the product of a length scale, ℓ , and a velocity scale, q_{sgs} . Since the most active of the unresolved scales are those closest to the cutoff, the natural length scale in LES modeling is the filter width, which is the size of the smallest structure in the flow, and is proportional to the grid size (the most commonly used ratio between filter width and grid size is 2). This convention, however, is not universally accepted and some authors absorb the factor of two into the constant of proportionality between the grid size and the length scale. For consistency the latter choice will be used in the following, and Δ will be the grid size (or an appropriate average in the case of anisotropic meshes) unless otherwise stated.

The velocity scale is usually taken to be the square-root of the trace of the SGS stress tensor, $q_{sgs}^2 = \tau_{kk}$. Although in some cases a transport equation is solved to determine q_{sgs}^2 (see below), in most cases the equilibrium assumption is made to simplify the problem further and obtain an algebraic model for the eddy viscosity.

The equilibrium assumption is based on the consideration that the small scales of motion have shorter time scales than the large, energy-carrying eddies; thus, it can be hypothesized that they

adjust more rapidly than the large scales to perturbations, and recover equilibrium nearly instantaneously. Under this assumption, the transport equation for q_{sgs}^2 , equation (2.18) which is of the form

$$\begin{aligned} \frac{\partial q_{sgs}^2}{\partial t} + \frac{\partial}{\partial x_j} (\bar{u}_j q_{sgs}^2) = & [\text{Turbulent transport}] + [\text{Pressure diff.}] \\ & + [\text{Viscous diff.}] + [\text{SGS diff.}] - 2\tau_{ij}\bar{S}_{ij} - 2\varepsilon \end{aligned} \quad (4.3)$$

simplifies significantly, since all terms drop out, except for the production term, $\varepsilon_{sgs} = \tau_{ij}\bar{S}_{ij}$, and for the viscous dissipation of SGS energy, ε , to yield:

$$-\tau_{ij}\bar{S}_{ij} = \varepsilon. \quad (4.4)$$

The equilibrium assumption implies inertial range dynamics: energy is generated at the large-scale level, and transmitted to smaller and smaller scales. All of the viscous dissipation takes place at the subgrid-scale level.

Very little testing of the applicability of this assumption to the small scales of turbulence is available. It is well known that in most flows of interest, the large scales are not in equilibrium: Smith and Yakhot (1993) studied the short-time behavior of the eddy viscosity in the Reynolds-averaged framework, and found that $K - \varepsilon$ models do not predict the correct response of the eddy viscosity if equilibrium turbulence is suddenly subjected to a perturbation (system rotation, for instance). The fact that a SGS model (the Smagorinsky model described in the next section), applied to the same problem, gave results in good agreement with their theory (Bardina *et al.* 1985), however, indicates that the small scales tend to equilibrium faster than the large ones, and thus satisfy the equilibrium assumption better than the large scales, or that, as long as the correct non-equilibrium response of the small scales is captured, the overall development of a turbulent flow may be predicted accurately. In more complex flows, in which extra strains, backscatter, intermittency and other phenomena play a role, it is not known whether the small scales would still be represented adequately by equilibrium-based models.

2. Smagorinsky model

The Smagorinsky model (1963) is, from an historical point of view, the progenitor of all subgrid-scale stress models, and is still in use. It is based on the equilibrium hypothesis, (4.4). If the viscous dissipation is modeled as $\varepsilon \sim q_{sgs}^3/\ell$, and (4.1) is substituted into (4.4) with $\nu_T \sim \ell q_{sgs}$, one obtains $q_{sgs} \sim \ell|\bar{S}|$, where $|\bar{S}| = (2\bar{S}_{ij}\bar{S}_{ij})^{1/2}$ is the magnitude of the strain-rate tensor. Letting $\ell \sim \Delta$, the eddy viscosity can be written

$$\nu_T = (C_s\Delta)^2|\bar{S}|. \quad (4.5)$$

Since the constant C_s (the Smagorinsky constant) is real, the model is absolutely dissipative: $\varepsilon_{sgs} = -(C_s\Delta)^2|\bar{S}|^3 \leq 0$.

To evaluate C_s , Lilly (1967) assumed the existence of an inertial range spectrum $E(k) = \alpha \varepsilon^{2/3} k^{-5/3}$. Then $|\bar{S}|$ can be evaluated approximately by integrating the enstrophy spectrum over all resolved wavenumbers

$$|\bar{S}|^2 \simeq 2 \int_0^{\pi/\Delta} k^2 E(k) dk = 2\alpha \varepsilon^{2/3} \int_0^{\pi/\Delta} k^{1/3} dk = \frac{3}{2} \alpha \varepsilon^{2/3} \left(\frac{\pi}{\Delta} \right)^{4/3}. \quad (4.6)$$

With $\alpha = 1.41$, this gives

$$C_s \simeq \frac{1}{\pi} \left(\frac{2}{3\alpha} \right)^{3/4} = 0.18. \quad (4.7)$$

In a previous article (Lilly 1966) the same constant had been evaluated analytically in terms of integrals of the velocity correlation function, assuming a second-order central discretization to approximate the velocity derivatives, and the value $C_s = 0.23$ was obtained.

Among the earliest applications of the Smagorinsky (1963) model to LES is the simulation of plane channel flow at infinite Reynolds number by Deardorff (1970). Finite differences were used to discretize the filtered equations of motion ($24 \times 21 \times 14$ grid points were employed); the value of the constant recommended by Lilly (1966) was found to damp the turbulent fluctuations excessively, and a lower value, $C_s = 0.1$, was preferred. Since the no-slip condition could not be used at the wall, approximate boundary conditions were applied to force the existence of logarithmic layer; the additional assumption was made that the turbulent fluctuations were isotropic. The boundary conditions applied by Deardorff (1970) were¹:

$$\frac{\partial^2 \bar{u}}{\partial y^2} = -\frac{1}{\kappa(\Delta y/2)^2} + \frac{\partial^2 \bar{u}}{\partial z^2} \quad (4.8)$$

$$v = 0 \text{ at the wall} \quad (4.9)$$

$$\frac{\partial^2 \bar{w}}{\partial y^2} = \frac{\partial^2 \bar{w}}{\partial x^2}. \quad (4.10)$$

Mean velocity and Reynolds stresses (Figure 4.1) were in acceptable agreement with the experimental data of Laufer (1951), and contours of turbulent fluctuations demonstrated forcefully that turbulence could be sustained in a simulation.

Clark *et al.* (1979) studied the application of LES to the decay of homogeneous isotropic turbulence *a priori*, by filtering explicitly the velocity field obtained from a direct simulation (DNS), and comparing the exact stresses to the modeled ones. They found that the stresses predicted by the Smagorinsky (1963) model correlate poorly with the exact ones, although the prediction of the global (volume-averaged) SGS dissipation is fairly accurate. McMillan *et al.* (1980) applied the same technique to the study of homogeneous shear flows, and obtained similar results; furthermore, they found that, in the presence of mean shear, the value of the constant C_s must be reduced by approximately a factor of two to match the mean square values of the modeled and exact stresses, a finding consistent with the calculations of Deardorff (1970).

¹Unless otherwise specified, in the following x or x_1 will indicate the streamwise direction, y or x_2 the wall-normal direction, and z or x_3 the spanwise direction; u , v and w (or u_1 , u_2 , and u_3) are the velocity components in the three coordinate directions, respectively.

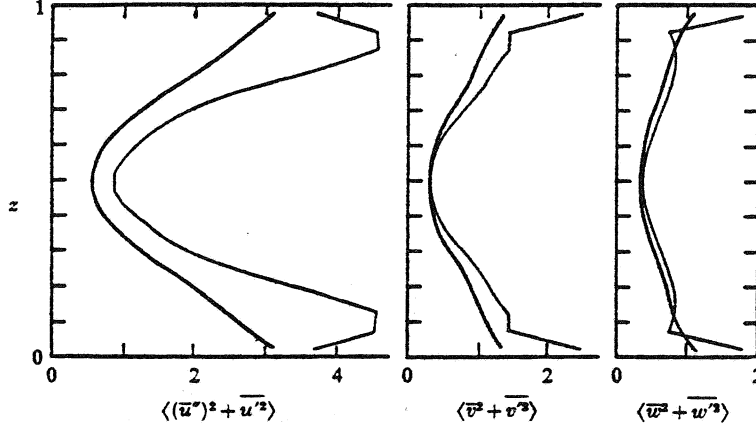


Figure 4.1: Normal Reynolds stress profiles (from Deardorff 1970). The wall-normal coordinate and velocity are z and w , respectively. Heavy curves: experiment.

Moin *et al.* (1978) and Moin and Kim (1982) were the first to perform the LES of a wall-bounded flow (plane channel flow) resolving the wall layer (thereby applying the no-slip conditions, rather than approximate wall boundary conditions). The calculations by Moin and Kim (1982) used Fourier expansions in the streamwise and spanwise direction, with $64 \times 63 \times 128$ grid points, to solve a low-Reynolds number ($Re_\tau = 640$) channel flow. They used a two-part model similar to that introduced by Schumann (1975) (see section 7) of the form:

$$\tau_{ij} = -2\nu_T (\bar{S}_{ij} - \langle \bar{S}_{ij} \rangle) - 2\nu_T^* \langle \bar{S}_{ij} \rangle; \quad (4.11)$$

The first term in (4.11) is a Smagorinsky term modified in order to eliminate the effect of the mean shear to model the SGS stresses as if the flow were isotropic:

$$\nu_T = \ell^2 \left[2 (\bar{S}_{ij} - \langle \bar{S}_{ij} \rangle) (\bar{S}_{ij} - \langle \bar{S}_{ij} \rangle) \right]^{1/2}, \quad (4.12)$$

while the second term,

$$\nu_T^* = \ell^{*2} \left[2 \langle \bar{S}_{ij} \rangle \langle \bar{S}_{ij} \rangle \right]^{1/2}, \quad (4.13)$$

is designed to account for the inhomogeneity due to the non-zero mean shear, and for the production of subgrid-scale energy in the near-wall region, where the grid resolution is inadequate. The length scale was modified by the introduction of Van Driest (1956) damping to account for the reduced growth of the small scales near the wall; the length scales ℓ and ℓ^* were given by

$$\ell = C_s \Delta [1 - \exp(-y^+/25)]; \quad \ell^* = 0.25 \Delta z [1 - \exp(-y^{+2}/25^2)]; \quad \Delta^3 = \Delta x \Delta y \Delta z, \quad (4.14)$$

and $C_s = 0.1$.

The results of the Moin and Kim (1982) simulation were in excellent agreement with experimental data. Comparison of the mean velocity and turbulence intensity profiles with the experimental data of Hussain and Reynolds (1975) are shown in Figures 4.2 and 4.3. The structure of turbulence in the near-wall layer (Moin 1984; Moin and Kim 1985; Kim and Moin 1986) was also captured

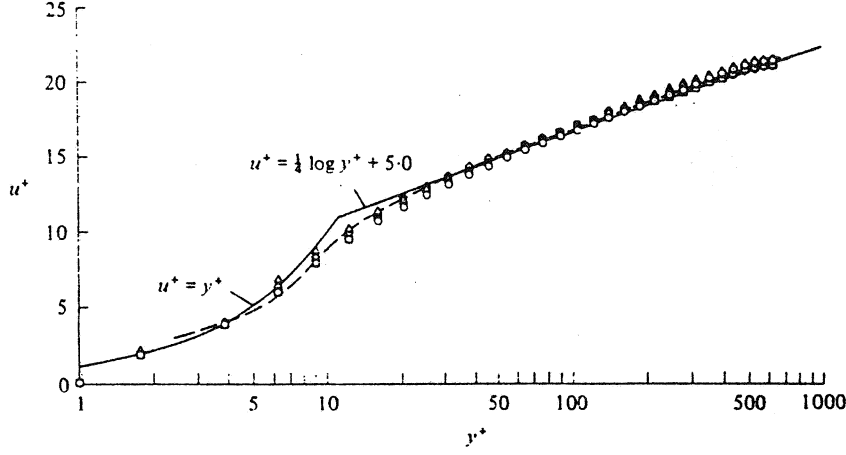


Figure 4.2: Mean velocity profile (from Moin and Kim 1982). Δ , \diamond , \square , \circ Computations; ——— experiment.

well. The low-speed streaks, for instance, had the correct length ($\lambda_x^+ \simeq 1,200$), although their spacing was high ($\lambda_z^+ \simeq 200$).

Horiuti (1987) showed that near the wall, if finite differences are used, the truncation error in the normal momentum equation is $o[(\Delta y_{j+1} - \Delta y_j) Re^2]$ when the rotational form of the Navier-Stokes equations is used, in which the advective term is written as

$$\frac{\partial}{\partial x_j} (\bar{u}_i \bar{u}_j) = \bar{u}_j \left(\frac{\partial \bar{u}_i}{\partial x_j} - \frac{\partial \bar{u}_j}{\partial x_i} \right) + \frac{1}{2} \frac{\partial}{\partial x_i} (\bar{u}_k \bar{u}_k). \quad (4.15)$$

For the stretched meshes used in the calculations by Moin and Kim (1982), the truncation error could be very large near the wall. Horiuti (1987) used the skew-symmetric scheme

$$\frac{\partial}{\partial x_j} (\bar{u}_i \bar{u}_j) = \frac{1}{2} \left[\bar{u}_j \frac{\partial \bar{u}_i}{\partial x_j} + \frac{\partial}{\partial x_j} (\bar{u}_i \bar{u}_j) \right], \quad (4.16)$$

and obtained more accurate prediction of turbulence statistics even using a coarser mesh than that employed by Moin and Kim (1982). The difference was most significant in the budget of the $\langle v^2 \rangle$ stress (Figure 4.4).

Other, more recent, applications of the Smagorinsky model include the study of transition in boundary layers and plane channel flow (Piomelli *et al.* 1990a; Piomelli and Zang 1991b), the simulations of the flow in a square duct (Madabushi and Vanka, 1991) and in a rotating channel (Tafti and Vanka, 1992). While the latter authors used a standard form of the Smagorinsky model, Piomelli and coworkers found that the Smagorinsky model overdamped the perturbations in the early stages of transition, leading to relaminarization even at supercritical Reynolds numbers. They introduced an intermittency function to reduce the SGS stresses in laminar flow.

The Smagorinsky model has been successful in predicting a number of simple flows, despite the poor correlation between actual and modeled stress, for a number of reasons: first, it predicts the integrated energy transfer to the small scales adequately, although it cannot predict backscatter,

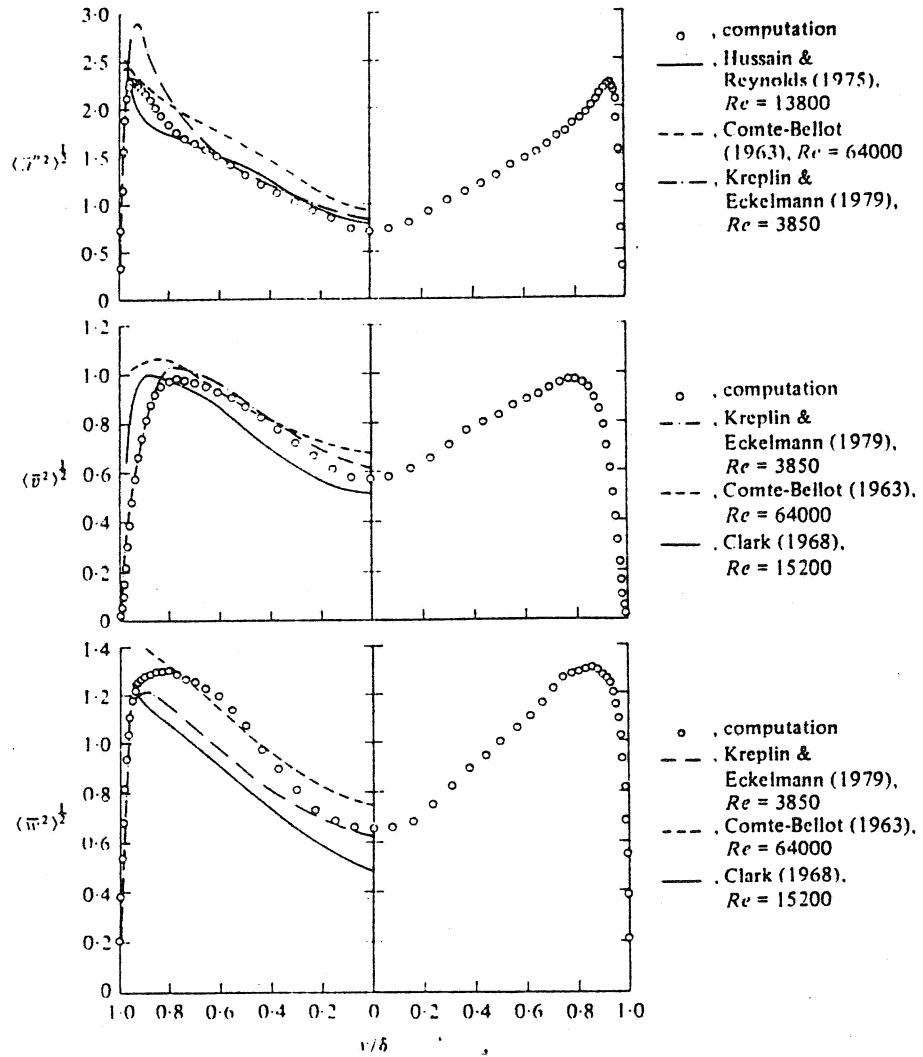


Figure 4.3: Turbulence intensities (from Moin and Kim 1982).

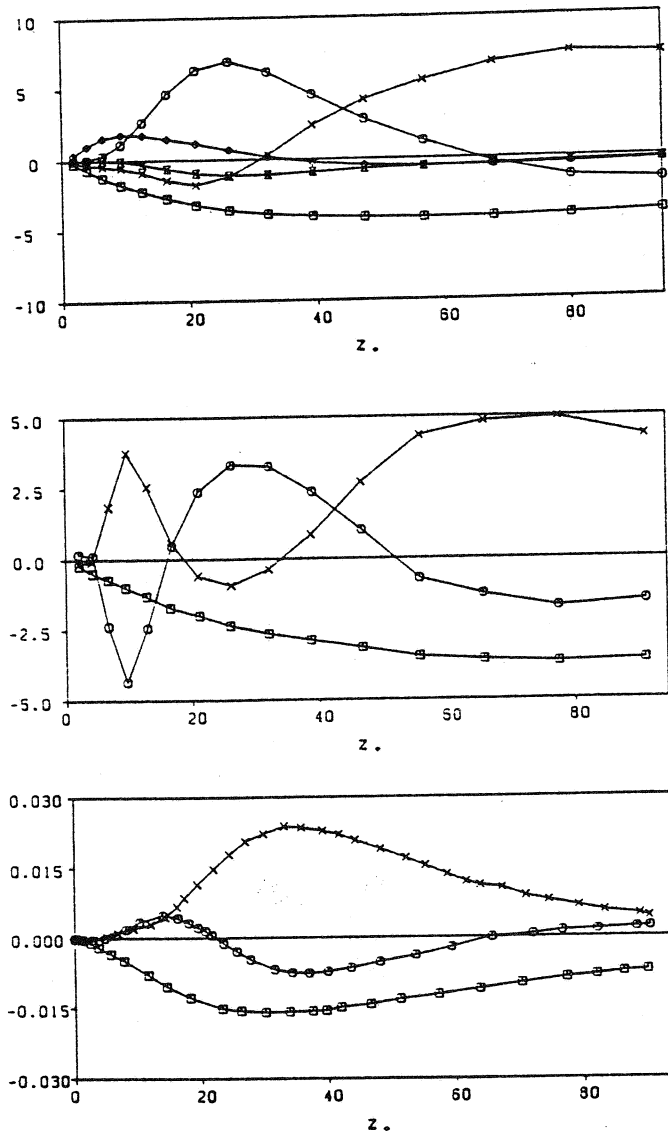


Figure 4.4: Wall-normal Reynolds stress budget (from Horiuti 1987). The wall-normal coordinate is z^+ . \circ Turbulent transport; \times velocity-pressure; \square dissipation. Top: Horiuti (1987); center: Moin and Kim (1982); bottom: Moser and Moin (1984) (DNS of curved channel flow, $Re_\tau = 180$).

nor the local energy transfer very well. Secondly, a number of *ad hoc* corrections have been introduced in the near-wall region and during transition from laminar to turbulent flow. Finally, only very simple, equilibrium flows have been computed using the Smagorinsky model. Its application to non-equilibrium turbulent flows has never been attempted, and in more complex geometries, involving separation, reattachment, strongly three-dimensional effects and so on, its performance might become inadequate. Furthermore, the fact that various *ad hoc* adjustments of the length scales were required indicates that the model cannot represent turbulent fields in sheared flows, in flows near solid walls or in transitional regimes with a single universal constant. Finally, it should be remarked that, if the Leonard stresses are computed [as they were in the calculations by Moin and Kim (1982) and Horiuti (1987)], the model is not Galilean invariant (Speziale 1985).

3. Two-point closures

Two-point closures have been an alternative way to derive SGS models. The results obtained by Kraichnan (1976) using the test field model (TFM) have been discussed in Chapter 2. Chollet and Lesieur (1981) used the Eddy-Damped, Quasi-Normal Markovian (EDQNM) theory to develop a SGS model with similar results. The Chollet–Lesieur (1981) model uses $[K_c E(K_c)]^{1/2}$ (where K_c is the cutoff wave number and $E(k)$ is the kinetic energy spectrum) as velocity scale, and K_c^{-1} as length scale for the eddy viscosity, which, in wave space, is given by

$$\hat{\nu}_T(k) = \hat{\nu}_T^+(k/K_c) [E(K_c)/K_c]^{1/2}, \quad (4.17)$$

where $\hat{\nu}_T^+(k/K_c)$ can be approximated by (Chollet 1985)

$$\hat{\nu}_T^+(x) = 0.267 + 9.21 \exp(-3.03/x). \quad (4.18)$$

Chollet and Lesieur (1981) simulated homogeneous isotropic turbulence and recovered the Kolmogorov spectrum. The model has subsequently been extended to anisotropic flows. Dang (1985) used it to simulate turbulence subjected to two successive plane strains, while Aupoix (1986) simulated the same experiment using the simplified EDQNM model of Cambon, Jeandel and Mathieu (1981).

Among the advantages of the Chollet–Lesieur model is that it produces zero eddy viscosity as long as there is no energy near the cutoff. This property has been exploited by Dang and Deschamps (1987), who computed laminar–turbulent transition in a plane channel. Its main disadvantage is the fact that it is defined in wave space, which hampers its extension to finite-difference schemes and to complex geometries. To overcome this shortcoming, Métais and Lesieur (1992) derived the “structure function model.” Assuming a cutoff wave number in the inertial region of a Kolmogorov spectrum, they expressed the energy spectrum at the cutoff, $E(K_c)$, in terms of the large-scale second-order velocity structure function,

$$\overline{F_2}(\mathbf{r}) = \langle [\bar{u}_i(\mathbf{x} + \mathbf{r}) - \bar{u}_i(\mathbf{x})] [\bar{u}_i(\mathbf{x} + \mathbf{r}) - \bar{u}_i(\mathbf{x})] \rangle, \quad (4.19)$$

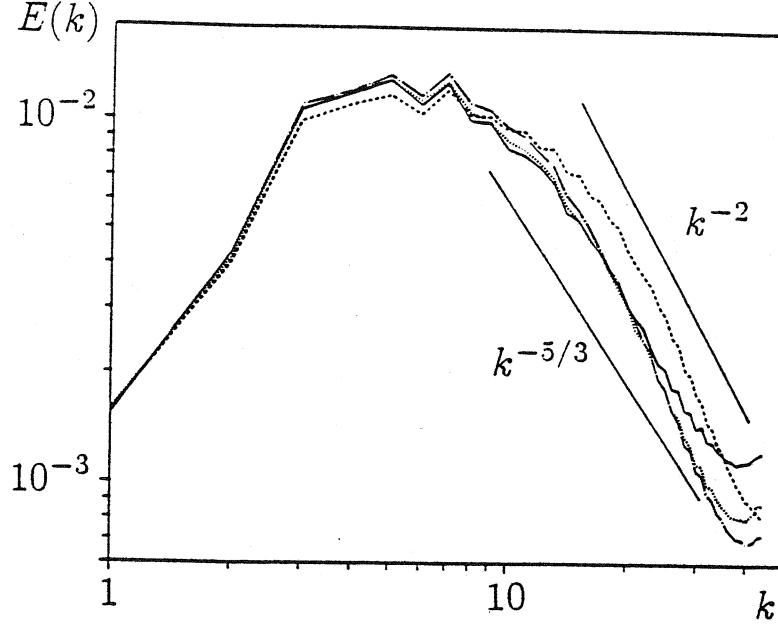


Figure 4.5: Kinetic energy spectrum $E(k)$ (from Métais and Lesieur 1992). — Structure function model; --- Chollet-Lesieur (1985); Chollet-Lesieur (1985), no cusp; —·— Smagorinsky, $C_s = 0.23$.

where $\langle \cdot \rangle$ is an appropriate spatial average, and obtained

$$\nu_T = 0.063\Delta \left[\overline{F_2}(\Delta) \right]^{1/2}. \quad (4.20)$$

This model was used for large eddy simulations of homogeneous isotropic turbulence with good success (Figure 4.5). It must be remarked that, if an isotropic grid is used, the structure function can be seen as a finite difference approximation of the velocity gradient tensor:

$$\begin{aligned} \overline{F_2} &= \langle [\overline{u_i}(\mathbf{x}, t) - \overline{u_i}(\mathbf{x} + \mathbf{r}, t)] [\overline{u_i}(\mathbf{x}, t) - \overline{u_i}(\mathbf{x} + \mathbf{r}, t)] \rangle \\ &\simeq 2\Delta^2 \frac{\partial \overline{u_i}}{\partial x_j} \frac{\partial \overline{u_i}}{\partial x_j} = 2\Delta^2 (\overline{S_{ij}} \overline{S_{ij}} + \xi_{ij} \xi_{ij}) = \Delta^2 (|\overline{\mathbf{S}}|^2 + \omega_i \omega_i), \end{aligned} \quad (4.21)$$

(where ξ_{ij} is the rotation tensor, and ω_i the vorticity), which gives

$$\nu_T(\mathbf{x}) = 0.063\Delta^2 \left(|\overline{\mathbf{S}}|^2 + |\boldsymbol{\omega}|^2 \right)^{1/2}. \quad (4.22)$$

Thus, the structure function model in its original form is actually a Smagorinsky-like model with the strain-rate replaced by the velocity gradient tensor. For isotropic flows, the model is less dissipative than the Smagorinsky model, in which the value $C_s = 0.23$ is commonly used. For sheared flows, however, in which the Smagorinsky constant is usually reduced to $C_s = 0.1$, the structure function is likely to be excessively dissipative.

Normand and Lesieur (1992) used a two-dimensional structure function (in which F_2 is evaluated by averaging only over planes parallel to the wall) to study transition in a compressible boundary

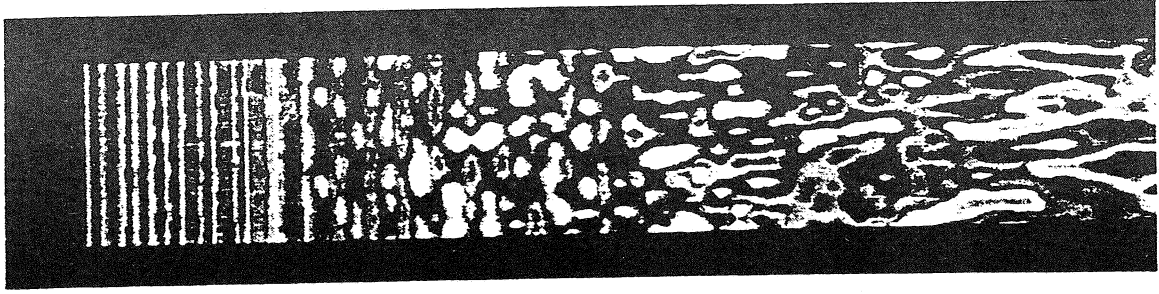


Figure 4.6: Streamwise velocity fluctuations (from Normand and Lesieur 1992).

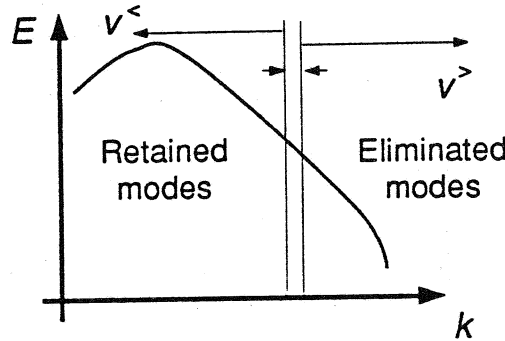


Figure 4.7: Wavenumber elimination in the ϵ -RNG procedure.

layer at Mach number $M = 0.5$ and 5 . In Figure 4.6 the streamwise velocity fluctuations are shown. The 2D formulation gave decreased dissipation, and the growth rates of the perturbation were overestimated by a factor of 2.

4. Renormalization Group theory

The renormalization group (RNG) theory of Yakhot and Orszag (1986) can be used to derive an algebraic subgrid stress model. The theory considers the incompressible motion of a fluid in an infinite domain stirred by a Gaussian random force. The force represents the effect of the large-scale features of the flow, namely the initial and boundary conditions, on the turbulent scales of motion. The theory is based on a recursive process: the wavenumbers in a narrow band $\Lambda < k < \Lambda + dk$ are eliminated from the equations for the velocity modes $k < \Lambda$ through an ensemble-average over the force field (Figure 4.7). This introduces a correction to the eddy viscosity, that can be determined from an ODE in which a parameter ϵ appears; the ODE is solved to lowest order in ϵ . To recover the Kolmogorov spectrum, however, requires $\epsilon = 4$. The procedure is repeated until a fixed point is reached at which the model does not change any longer. The ϵ -RNG procedure results in a total viscosity, $\nu_{tot} = \nu + \nu_T$, given by

$$\nu_{tot} = \nu \left[1 + H \left(\frac{\nu_s^2 \nu_{tot}}{\nu^3} - C \right) \right]^{1/3}, \quad (4.23)$$

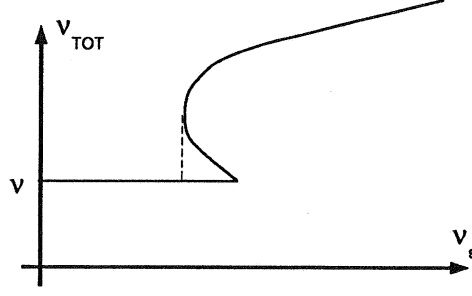


Figure 4.8: Locus of the solution of the cubic and the quartic in the RNG subgrid-scale stress model.

where $\nu_s = (c_{rng}\Delta)^2 |\bar{S}|$, and $H(x)$ is a Heavyside ramp function. The coefficients $c_{rng} = 0.157$,² and $C = 100$ are obtained from the theory, without need for *ad hoc* adjustments. If $\nu_s \simeq 0$, the argument of the ramp function is negative and the total viscosity is equal to the molecular one. Thus, in low-Reynolds number flows (near the wall or during laminar-turbulent transition) the modeled eddy viscosity vanishes without the need for *ad hoc* wall damping or intermittency functions. In turbulent regions of the flow, $\nu_s \gg \nu$ and $\nu_{tot} \simeq \nu_s$, returning the Smagorinsky model.

In practice, however, several *ad hoc* adjustments are used (A. Yakhot *et al.* 1989). The original formulation contained a term $\nu_s^2 \nu_{tot} / \nu^3$ in the argument of the ramp function that gave multiple solutions for ν_{tot} for a range of values of ν_s (Figure 4.8). To avoid the unphysical roots, a quartic is solved in which $\nu_s^2 \nu_{tot}^2 / \nu^3 \nu_{tot}$ replaces $\nu_s^2 \nu_{tot} / \nu^3$. Solution of the quartic, however, gives rise to a discontinuity in the total viscosity (Lund, 1990). The model used by A. Yakhot *et al.* (1989) also contained other *ad hoc* modifications: the total viscosity was

$$\nu_{tot} = \nu \left[1 + H \left(\frac{\nu_s^2 \nu_{tot}^2}{\nu^3 \nu_{tot}} - C \right) \right]^{1/3}, \quad (4.24)$$

where

$$\nu_s = (\gamma_{rng} \gamma_{iso})^{1/2} \Lambda^{-2} |\bar{S}|, \quad (4.25)$$

$$\gamma_{iso} = \frac{3v^2}{u^2 + v^2 + w^2}, \quad (4.26)$$

$\gamma_{rng} = 0.1195$, and Λ is an inverse length scale also evaluated by using the RNG theory to eliminate all scales smaller than the cutoff in a manner that accounts properly for grid anisotropy. The *ad hoc* factor γ_{iso} is introduced to account for the anisotropy of the flow in the near-wall region. The RNG eddy viscosity, however, goes to zero near the wall with an incorrect asymptotic behavior. Yakhot *et al.* (1989) applied this model to LES of turbulent channel flow, obtaining results in fair agreement with DNS and experimental data.

Piomelli *et al.* (1990b) used the RNG model (4.23) to study forced transition in a flat-plate boundary layer. They used a standard form of the length scale (including Van Driest damping),

²Yakhot and Orszag obtain a value $c_{rng} = 0.0787$ using a filter width that is twice the grid size.

rather than the one employed by Yakhot *et al.* (1989), and found that, although transition could be predicted accurately, the results were very much grid-dependent. Since the argument of the ramp function depends on the eighth power of the filter width Δ , changes in the grid size have a very strong effect on the location of the transition process where the eddy viscosity first becomes non-zero. In particular, it was found that the onset of transition was predicted correctly using $16 \times 33 \times 26$ grid points, but that when the grid was refined, the eddy viscosity remained equal to zero too long, leading to the incorrect prediction of the late stages of transition. The channel flow calculations of Zang and Piomelli (1993) show that the RNG model does not predict the drag crisis accurately. Karniadakis *et al.* (1993a) have applied the RNG model (4.24) to the flow on a backward facing step and Karniadakis and Orszag (1993b) have used it for the calculation of the wake of a sphere.

5. Dynamic models

Dynamic modeling of the subgrid-scale stresses was introduced by Germano *et al.* (1991). In models of this type, the model coefficients are computed dynamically as the calculation progresses rather than imposed *a priori* based on the energy content of the smallest resolved scale. The dynamic eddy viscosity model of Germano *et al.* (1991) is based on the introduction of two filters; in addition to the *grid* filter (denoted by an overbar), which defines the resolved and subgrid scales, a *test* filter (denoted by a circumflex) is used, whose width is larger than the grid filter width. The stress terms that appear when the grid filter is applied to the Navier-Stokes equations are the subgrid-scale (SGS) stresses τ_{ij} ; in an analogous manner, the test filter defines a new set of stresses, the subtest-scale stresses T_{ij} . The resolved turbulent stresses, $\mathcal{L}_{ij} \equiv \overline{\widehat{u_i u_j}} - \widehat{u_i} \widehat{u_j}$, which represent the contribution of the smallest resolved scales to the Reynolds stresses, can be computed from the large-scale velocity; they are related to the SGS stresses, τ_{ij} , by the identity (Germano 1992)

$$\mathcal{L}_{ij} \equiv T_{ij} - \widehat{\tau}_{ij}, \quad (4.27)$$

where $T_{ij} \equiv \widehat{\widehat{u_i u_j}} - \widehat{u_i} \widehat{u_j}$ are the subtest-scale stresses.

The subgrid- and subtest-scale stresses are then parameterized by eddy viscosity models of the form (4.1):

$$\tau_{ij} - \frac{\delta_{ij}}{3} \tau_{kk} = -2C \overline{\Delta}^2 |\overline{S}| \overline{S}_{ij} = -2C \beta_{ij}, \quad (4.28)$$

$$T_{ij} - \frac{\delta_{ij}}{3} T_{kk} = -2C \widehat{\Delta}^2 |\widehat{S}| \widehat{S}_{ij} = -2C \alpha_{ij}. \quad (4.29)$$

Substituting (4.28) and (4.29) into (4.27) yields

$$\mathcal{L}_{ij}^a = \mathcal{L}_{ij} - \frac{\delta_{ij}}{3} \mathcal{L}_{kk} = -2C \alpha_{ij} + 2C \widehat{\beta}_{ij}. \quad (4.30)$$

This is a set of five independent equations that cannot be solved explicitly for C , which appears inside a filtering operation. If, however, one assumes that $C = C(y, t)$, then $\widehat{C \beta_{ij}} = C \widehat{\beta}_{ij}$. To

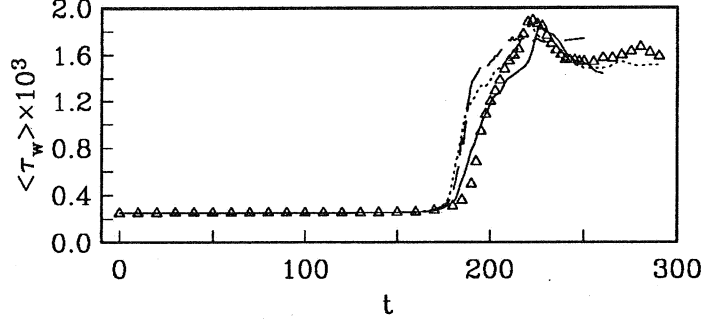


Figure 4.9: Time evolution of the wall shear (from Zang and Piomelli 1993). Scaled Smagorinsky model (Piomelli and Zang 1991b); --- RNG model; — dynamic eddy viscosity model (Germano *et al.* 1991); Δ fine direct simulation (Zang *et al.* 1990).

obtain a single coefficient from the five independent equations, furthermore, Germano *et al.* (1991) contracted both sides of (4.30) with \bar{S}_{ij} to yield

$$C = -\frac{1}{2} \frac{\langle \mathcal{L}_{kl} \bar{S}_{kl} \rangle}{\langle (\alpha_{mn} - \widehat{\beta}_{mn}) \bar{S}_{mn} \rangle}; \quad (4.31)$$

The SGS stresses given by (4.28) with C given by (4.31) vanish in laminar flows and at solid boundaries, and have the correct asymptotic behavior in the near-wall region without damping functions or intermittency factors; the model can also be formulated in real space or adapted to finite-difference calculations. Furthermore, the model is capable of providing backscatter. It was used by Germano *et al.* (1991) for LES of transitional and fully-developed turbulent channel flows, in which it gave more accurate results than either the Smagorinsky or the RNG model in the formulation of Piomelli *et al.* (1990b). The time development of the wall stress τ_w in fundamental transition in plane channel flow is shown in Figure 4.9, taken from Zang and Piomelli (1993); the results of the dynamic model compare very well with the DNS of Zang *et al.* (1990); the dynamic model produces an overshoot in the wall shear stress that agrees well with the actual one, and also gives reasonable agreement for the time-averaged wall shear stress in the fully turbulent state. The peak wall shear stress computed with the dynamic model is within 3% of the DNS prediction. The RNG model does not perform as well in either of these respects.

The model (4.28)-(4.31) was extended to compressible flows by Moin, Squires, Cabot and Lee (1991), who tested the compressible extension both *a priori* and *a posteriori* in the LES of isotropic turbulence. They examined two cases: an almost incompressible one and one with high turbulent Mach number. The LES results compared well with the DNS in both cases.

Lilly (1992), proposed to minimize the sum of the squares of the residual,

$$E_{ij} = \mathcal{L}_{ij}^a + 2C\alpha_{ij} - 2C\widehat{\beta}_{ij}, \quad (4.32)$$

by contracting both sides of (4.30) with $\alpha_{ij} - \widehat{\beta}_{ij}$ to yield:

$$C(y, t) = -\frac{1}{2} \frac{\langle \mathcal{L}_{ij}^a (\alpha_{ij} - \widehat{\beta}_{ij}) \rangle}{\langle (\alpha_{mn} - \widehat{\beta}_{mn})(\alpha_{mn} - \widehat{\beta}_{mn}) \rangle}. \quad (4.33)$$

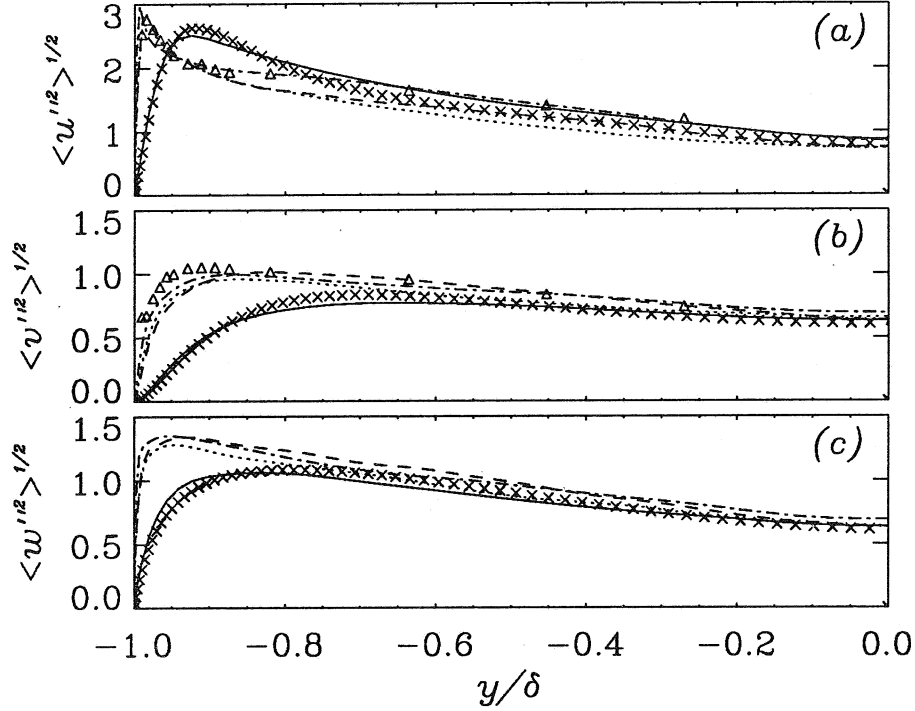


Figure 4.10: Turbulence intensities (from Piomelli 1993). — $Re_\tau = 200$; $Re_\tau = 1,000$, fine mesh; --- $Re_\tau = 1,000$, coarse mesh; -·- $Re_\tau = 2,000$; \times DNS (Kim *et al.* 1987); \triangle experiment (Wei and Willmarth 1989). (a) u'' ; (b) v'' ; (c) w'' .

The least-squares minimization has been used by Piomelli (1993) to compute the flow in a plane channel at Reynolds numbers in the range $Re_\tau = 200 - 2,000$. The results were in very good agreement with DNS and experimental data. The rms turbulence intensities, shown in Figure 4.10, exhibited no loss of accuracy in the near-wall region even at the highest Reynolds number. The location and magnitude of the peak streamwise turbulence intensity are predicted correctly even in the low-resolution calculation. Higher moments, such as the skewness factor of the large-scale velocity, shown in Figure. 4.11, also were in good agreement with the data. The skewness of w is nearly zero, as required by the spanwise symmetry of the flow; the skewness of v is in good agreement with DNS and experimental data; it is negative for $5 < y^+ < 30$, reflecting the presence of strong negative v motions there. The skewness of u requires some discussion; the low Reynolds number, high resolution case is in good agreement with the DNS data, and cases 2 and 3 are in good agreement with the experimental data for $y^+ > 20$. With increasing Reynolds number $S(u)$ increases, and the region where $S(v)$ is negative moves away from the wall, trends also observed in the experiments.

Among the other applications of the dynamic eddy viscosity model are the study of relaminarizing sink flow (Esmaili and Piomelli 1993), and the study of rotating turbulence by Squires and Piomelli (1994). In both of these cases the model gave predictions in good agreement with the

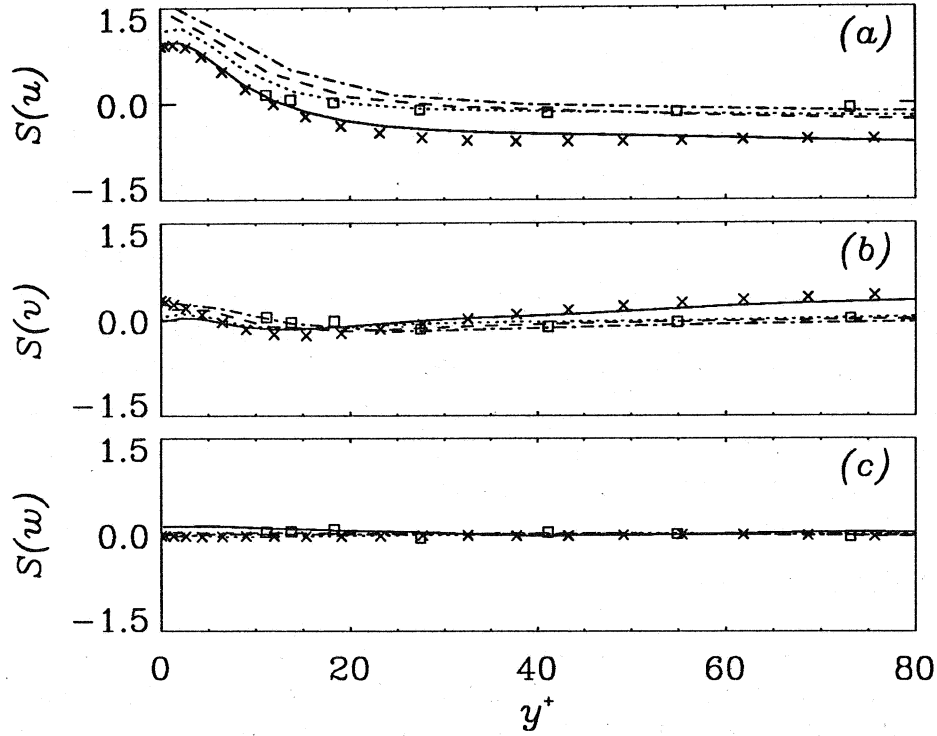


Figure 4.11: Skewness factor in wall coordinates (from Piomelli 1993). — $Re_\tau = 200$; $Re_\tau = 1,000$, fine mesh; --- $Re_\tau = 1,000$, coarse mesh; -.- $Re_\tau = 2,000$; \times DNS (Kim *et al.* 1987); \square experiment (Balint *et al.* 1991). (a) $S(u)$; (b) $S(v)$; (c) $S(w)$.

experimental data. The model coefficient was found to respond to perturbations from equilibrium in a realistic way and with the proper time scales.

A limitation of the dynamic model is, however, the plane averaging mentioned above. For flows in which no homogeneous directions exist, the model coefficient should be a function of all spatial coordinates. Even flows that are homogeneous in planes parallel to the wall may be intermittent, in which case the eddy viscosity should be non-zero only in regions of significant turbulent activity, and zero elsewhere, a behavior that is not always possible if plane averaging is performed. Although straightforward localization of the dynamic model gives rise to the problems mentioned above, it has nonetheless been used by Zang and coworkers (1993a) in simulations of the turbulent flow in a driven cavity. They performed some local averaging (over the test filter cell) and also constrained the total viscosity (sum of molecular and eddy viscosity) to be non-negative, thus allowing a small amount of backscatter. Since large (positive and negative) values of the eddy viscosity were observed only in the corner of the cavity, probably due to the low Reynolds number of the flow they studied, neither the local averaging nor the cutoff applied to avoid backscatter affected the results appreciably. In later work (Zang *et al.* 1993b) the same authors adopted a mixed model that was also localized in a similar manner. Ghosal and coworkers (1993) recast the problem in variational form, obtaining an integral equation for C that was solved iteratively. This removed the mathematical inconsistency, but the overhead associated with the iterative solution of the integral equation could be significant. The ill-conditioning that led to locally large values of C was removed by the integral formulation, and negative values of the model coefficient were avoided by the additional constraint that $C \geq 0$. This model was used for the LES of isotropic decay and to study the flow over a backward-facing step (Akselvoll and Moin 1993), with results in good agreement with DNS data.

6. Scale-similar models

Scale-similar models are based on the assumption that the most active subgrid scales are those closer to the cutoff, and that the scales with which they interact most are those right above the cutoff (Bardina *et al.* 1980, 1983). The “largest subgrid scales” can be obtained by filtering the SGS velocity $u'_i = u_i - \bar{u}_i$ to obtain

$$\overline{u'_i} = \bar{u}_i - \bar{\bar{u}}_i. \quad (4.34)$$

The cross stresses and SGS Reynolds stresses can then be written as

$$C_{ij} = \overline{u'_i u'_j} + \overline{u_j u'_i} \sim \bar{\bar{u}}_i \bar{\bar{u}}_j + \bar{\bar{u}}_j \bar{\bar{u}}_i \quad (4.35)$$

$$R_{ij} = \overline{u'_i u'_j} \sim \bar{u}'_i \bar{u}'_j; \quad (4.36)$$

substituting (4.34) into the equations above, and adding a Smagorinsky model to represent the dissipative effect of the small scales, gives the mixed model

$$\tau_{ij} - \frac{\delta_{ij}}{3} \tau_{kk} = C_B \left[\overline{u_i u_j} - \bar{\bar{u}}_i \bar{\bar{u}}_j - \frac{\delta_{ij}}{3} (\overline{u_k u_k} - \bar{\bar{u}}_k \bar{\bar{u}}_k) \right] - 2\nu_T \bar{S}_{ij}. \quad (4.37)$$

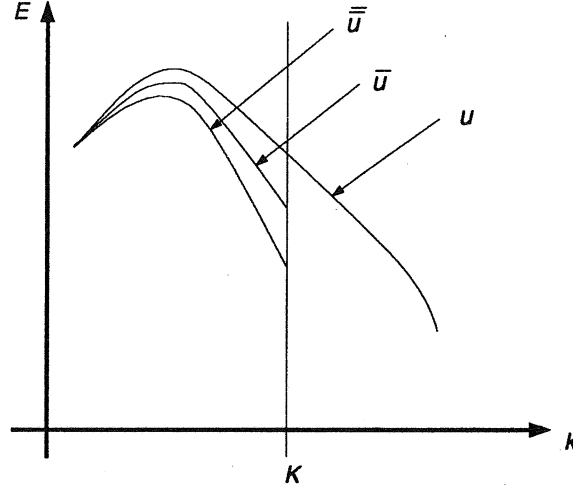


Figure 4.12: Spectra of the unfiltered, filtered and twice-filtered velocities.

The first part of the model, the scale-similar model, is non dissipative; if the Leonard stresses are computed, Galilean invariance is recovered if $C_B = 1$ (Speziale 1985) (the Smagorinsky model by itself is not Galilean invariant in that case). Numerical tests had given an optimum coefficient $C_B = 1.1$, very close to the theoretical value.

Bardina *et al.* (1980, 1983) applied the mixed model (4.37) to the simulation of homogeneous isotropic turbulence, obtaining improved results over the Smagorinsky model. Furthermore, they found that the modeled stresses are very highly correlated with the exact ones (the correlation coefficient was close to 1, versus 0.1–0.3 for the Smagorinsky model).

Piomelli *et al.* (1988) applied the mixed model to the calculation of plane channel flow at Reynolds numbers in the range $Re_\tau = 180 - 640$. The wall layer was resolved in their calculations, that used the same numerical approach as the earlier Moin and Kim (1982) simulation, but wrote the nonlinear term in skew-symmetric form. They found that the choice of model must be coupled with that of the filter, and that an inconsistent choice gives inaccurate results. When the Gaussian filter is used and the Leonard stresses are computed, for instance, inclusion of the scale-similar part of the model recovers Galilean invariance and gives more accurate results than the Smagorinsky part alone. When the Fourier cutoff filter is used, on the other hand, the scale-similar part of the model is identically zero, as are the Leonard stresses, and the Smagorinsky model alone is consistent and gives satisfactory results. Mean velocity (Figure 4.13), turbulence intensities and velocity spectra (Figure 4.14) were compared, and the agreement between filtered DNS data and LES results was very good. The mean streak spacing was also predicted accurately, although a coarser mesh was used than the one employed by Moin and Kim (1982). Horiuti (1989) observed that the major role of the scale-similar part of the model is to provide the backscatter of SGS energy.

A compressible version of the mixed model has been developed by Speziale *et al.* (1988), and applied by Zang *et al.* (1992) to the decay of compressible isotropic turbulence. They investigated the effect of the model constants on the results, and found that the constants recommended by

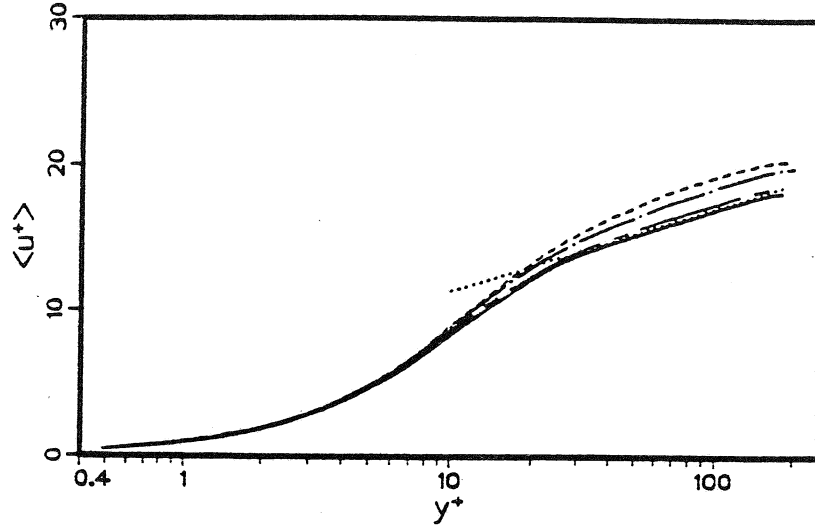


Figure 4.13: Mean velocity profiles (from Piomelli *et al.* 1988). Gaussian filter, mixed model. --- Very coarse grid; -.- coarse grid; fine grid; — DNS.

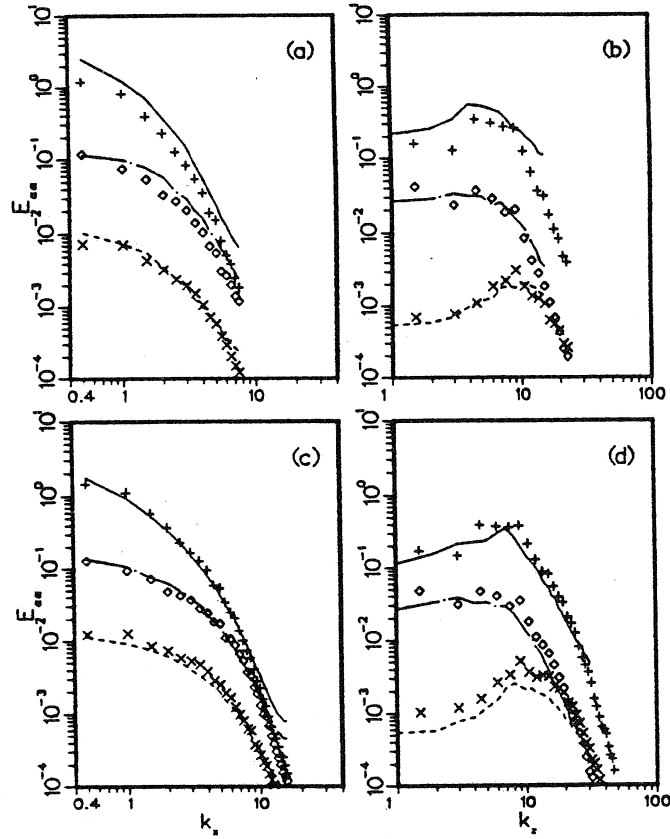


Figure 4.14: One-dimensional spectra (from Piomelli *et al.* 1988). Gaussian filter, mixed model, $y^+ = 12.93$. Lines: LES; symbols: DNS. —, + : u . ---, x : v , o : w . Left: streamwise; right: spanwise. Top: coarse grid; bottom: fine grid.

Speziale *et al.* (1988) gave good agreement with DNS data for the evolution of the compressible component of the kinetic energy and other compressible quantities.

A dynamic model including a scale-similar part has been applied by Zang *et al.* (1993b) to the calculation of flow in a driven cavity. They found that the inclusion of the scale-similar part reduced the contribution of the Smagorinsky part (and, therefore, the value of the coefficient) substantially, and that the model was better behaved, numerically, than the original formulation. The fact that they did not resolve the mathematical inconsistency may, however, have affected their results. The low Reynolds number of their simulations, moreover, did not allow the eddy viscosity to be significant except in small regions of the flow.

In summary, mixed models have given very satisfactory results in calculations that used the Gaussian filter. In finite-difference calculations, the second filtering operation is not trivial or unique, and fewer calculations have been performed that use such models. In general, one can say that the principle behind scale-similar models is to extrapolate the behavior of the scales below the cutoff based on the scales right above it, a concept that has theoretical support in the findings of Domaradzki *et al.* (1993, 1994). The difficulty of applying those models in non-spectral calculations has, however, limited the number of their applications.

7. One-equation models

One-equation models solve a transport equation for the subgrid-scale energy $\mathcal{K}_{sgs} = q_{sgs}^2/2$ to obtain the velocity scale. The terms in (2.18) that require modeling are the turbulent transport (term VIII) and pressure diffusion (term IX), which are usually modeled jointly as an added diffusion, and the viscous dissipation (term XII), which is usually taken to be proportional to $\mathcal{K}_{sgs}^{3/2}/\Delta$. Consequently, a one-equation model can be cast in the form

$$\nu_T = C_\nu \mathcal{K}_{sgs}^{1/2} \Delta \quad (4.38)$$

$$\begin{aligned} \frac{\partial \mathcal{K}_{sgs}}{\partial t} + \frac{\partial}{\partial x_j} (\mathcal{K}_{sgs} \bar{u}_j) &= + \frac{\partial}{\partial x_j} \left[\left(C_k \mathcal{K}_{sgs}^{1/2} \Delta + \nu \right) \frac{\partial \mathcal{K}_{sgs}}{\partial x_j} + \tau_{ij} \bar{u}_i \right] \\ &\quad - C_\epsilon \frac{\mathcal{K}_{sgs}^{3/2}}{\Delta} - \tau_{ij} \bar{S}_{ij}. \end{aligned} \quad (4.39)$$

Lilly (1967) assumed a Kolmogorov spectrum to evaluate the constants. Integration of the enstrophy spectrum yields $C_\epsilon = 0.93$, while requiring that the Smagorinsky model be recovered in equilibrium turbulence, in which $\tau_{ij} \bar{S}_{ij} = -C_\epsilon (\mathcal{K}_{sgs}^{3/2}/\Delta)$, gives

$$\nu_T = C_\nu \sqrt{\frac{C_\nu}{C_\epsilon}} \Delta^2 |\bar{S}| = C_s^2 \Delta^2 |\bar{S}| \quad (4.40)$$

to yield $C_\nu = 0.094$. The diffusion term was neglected.

One of the earliest applications of LES that used this model was the work of Schumann (1975), who performed an LES calculation of the flow in a plane channel and in an annulus at Reynolds number $Re_\tau = 5,900$ (based on friction velocity, $u_\tau = (\tau_w/\rho)^{1/2}$ and channel halfwidth, δ), using

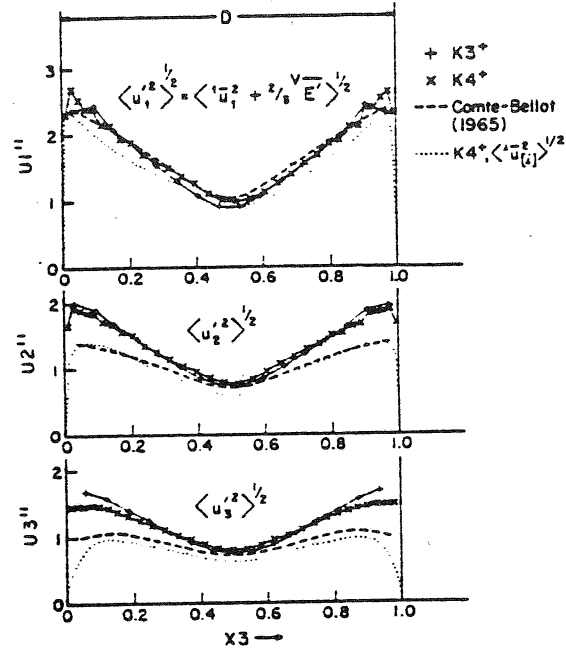


Figure 4.15: Turbulence intensities profiles (from Schumann 1975). The wall-normal coordinate and velocity are x_3 and u_3 , respectively. Resolved part; +, x, total; --- experimental data.

$64 \times 17 \times 32$ and $64 \times 33 \times 32$ grid points. The filtered Navier-Stokes equations were recast in a finite volume formulation. Both his SGS stress model and the approximate boundary conditions he used were more sophisticated than those employed by Deardorff, resulting in better agreement with the experimental data (Figure 4.15). He used a two-part model of the same form as the one used later by Moin and Kim (1982), given by Equations (4.11–4.14); a transport equation of the form (4.39), derived based on dimensional analysis and phenomenological arguments, was solved to obtain the SGS velocity scale. The values of the constants used, following Lilly (1967), were $C_\epsilon \simeq 0.9$, $C_\nu = 0.09$; he used a turbulent Prandtl number of 0.3 to obtain $C_k = 0.024$. In his simulation, the near-wall region was modeled. The wall stress was related to the velocity in the core by

$$\tau_{12} = \frac{\langle \tau_w \rangle}{\langle \bar{u}(x, y_2, z) \rangle} \bar{u}(x, y_2, z) \quad (4.41)$$

$$v = 0 \text{ at the wall} \quad (4.42)$$

$$\tau_{32} = \frac{1}{Re_\tau} \frac{\bar{w}(x, y_2, z)}{\Delta y/2}. \quad (4.43)$$

These equations, in which the subscript 2 refers to the first grid point off the solid wall, impose that the wall stress is proportional to the velocity at the first grid point (both in the streamwise and spanwise directions). The mean stress $\langle \tau_w \rangle$ can be known for a given pressure gradient, or can be calculated iteratively, by requiring that the plane-averaged velocity at the first grid point,

$\langle \bar{u}(x, y_2, z) \rangle$ satisfy the logarithmic law (Grötzbach, 1981). Grötzbach (1981) used an approach similar to that of Schumann (1975) to calculate turbulent flows in the presence of heat transfer.

Yoshizawa (1982) used the two-scale direct-interaction (DI) theory to derive an equation similar to (4.39). The constants he obtained were $C_\epsilon = 0.95$ and $C_\nu = 0.093$, consistent with Lilly's (1967) results. His model was used by Horiuti and Yoshizawa (1985) for the LES of turbulent channel flow. They used $C_k = 0.1$, and found that the one-equation model gave more accurate results when very coarse grids were used; on finer grids, however, there was little difference between the one-equation and the Smagorinsky model results.

Recently, a dynamic one-equation model has been developed by Ghosal *et al.* (1993) in which the coefficients C_ν , C_ϵ and C_k are computed at each time step by imposing identities of the same form as (4.27) and involving the solution of integral equations. Although the model in theory can give a more physical description of the energy transfer to and from the subgrid scales, and account for backscatter more accurately, to date its results do not compare favorably with the algebraic dynamic model.

One-equation models have several disadvantages: first, the expense involved in solving an additional equation does not seem to be justified by improvements in the accuracy. Furthermore, the "dissipation of SGS energy" is usually taken to be proportional to q_{sgs}^3/Δ . An unpublished *a priori* study by the author indicates that this assumption is extremely poor in channel flows. Finally, in laminar flows the right-hand side of the transport equation vanishes identically; this implies that, if the initial condition of a calculation consists of a large-scale perturbation (which does not contribute to the SGS energy) superimposed on a laminar profile, the subgrid-scale energy will remain equal to zero throughout the calculation, unless the flow is linearly unstable, in which case the roundoff error will eventually generate some SGS disturbance.

8. Wall layer models

As mentioned in Chapter 3, wall layer models (or approximate boundary conditions) allow one to bypass the near-wall region altogether, with considerable savings in terms of numerical resolution, by estimating the wall stress based on the velocity in the outer flow. A review of approximate boundary conditions used in the past can be found in Piomelli *et al.* (1989); usually, the first computational point is located in the logarithmic region, and the wall stress, which is required as a boundary condition to close the system, is expressed as a function of the velocity at the first grid point, through generalized forms of the law-of-the-wall, with empirical corrections to account for the topology of the near-wall structures.

The approximate boundary conditions used by Deardorff (1970) and Schumann (1975) have been mentioned before. Mason and Callen (1986) required that the logarithmic law be satisfied locally and instantaneously at the first grid point, an assumption based on local equilibrium of the near-wall region, that depends on the size of the averaging volume (the grid cell), and may not be valid for flows more complex than the standard boundary layer or plane channel.

Piomelli *et al.* (1989) applied conditions similar to (4.41–4.43); however, they required that the wall stress be correlated to the instantaneous velocity some distance downstream of the point where

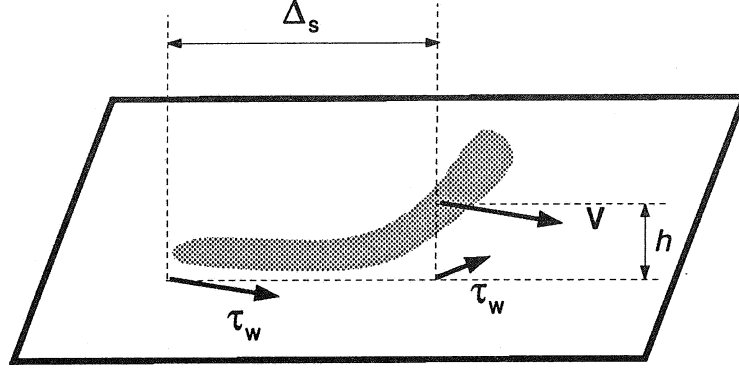


Figure 4.16: Shifted boundary condition

the wall stress is required, to take into account the inclination of the elongated structures in the near-wall region (Figure 4.16). Furthermore, they obtained the wall stress by solving iteratively a generalized law-of-the-wall that was also valid for flows with transpiration. This changes yielded improved results over Schumann's original (1975) model. The shifted model described above has been recently applied by Balaras *et al.* (1994) to the calculation of the flow in a plane channel at high Reynolds number, in calculations that used the dynamic SGS model, with results in excellent agreement with experimental data (Figure 4.17).

An alternative class of approximate boundary conditions that has shown much promise in preliminary studies is based on the use of Linear Stochastic Estimation (LSE) to obtain the wall stress. A linear estimate $\hat{\tau}_{w,i}(x, z)$ of the conditional average of the wall stress, given the velocity on the first grid plane as a condition, can be written as

$$\hat{\tau}_{w,i}(x, z) = \langle \tau_{w,i}(x, z) \mid \bar{u}_i(x, y_e, z) \rangle = L_{ij} * u_j(x, y_e, z), \quad (4.44)$$

where L_{ij} is a coefficient matrix obtained using the two-point correlations, $*$ denotes a convolution integral, and y_e is the first grid plane, where the velocity is computed. This technique has been applied successfully (see, for instance, Bagwell *et al.* 1993 and Bagwell 1994) to the study of plane channel flow, giving very accurate prediction of the statistics (Figure 4.18); it requires that the full two-point correlation tensor be known a priori (i.e., from experiment or previous direct simulations). While this requirement might seem unrealistic, recent results indicate that, if the correlations are known at a given Reynolds number, scaling arguments (Naguib and Wark 1993) may be invoked to use them at different Reynolds numbers.

Although approximate boundary conditions have been successful in simple, quasi-equilibrium flows, they do not seem applicable to complex turbulent flows, with extra gradients and other non-equilibrium features, unless significant progress is made in their development. The present generation of wall layer models probably requires too much semi-empirical information to be known *a priori* (law-of-the-wall, inclination of the near-wall structures, two-point correlations) to be useful if LES is to be a predictive, rather than postdictive, tool.

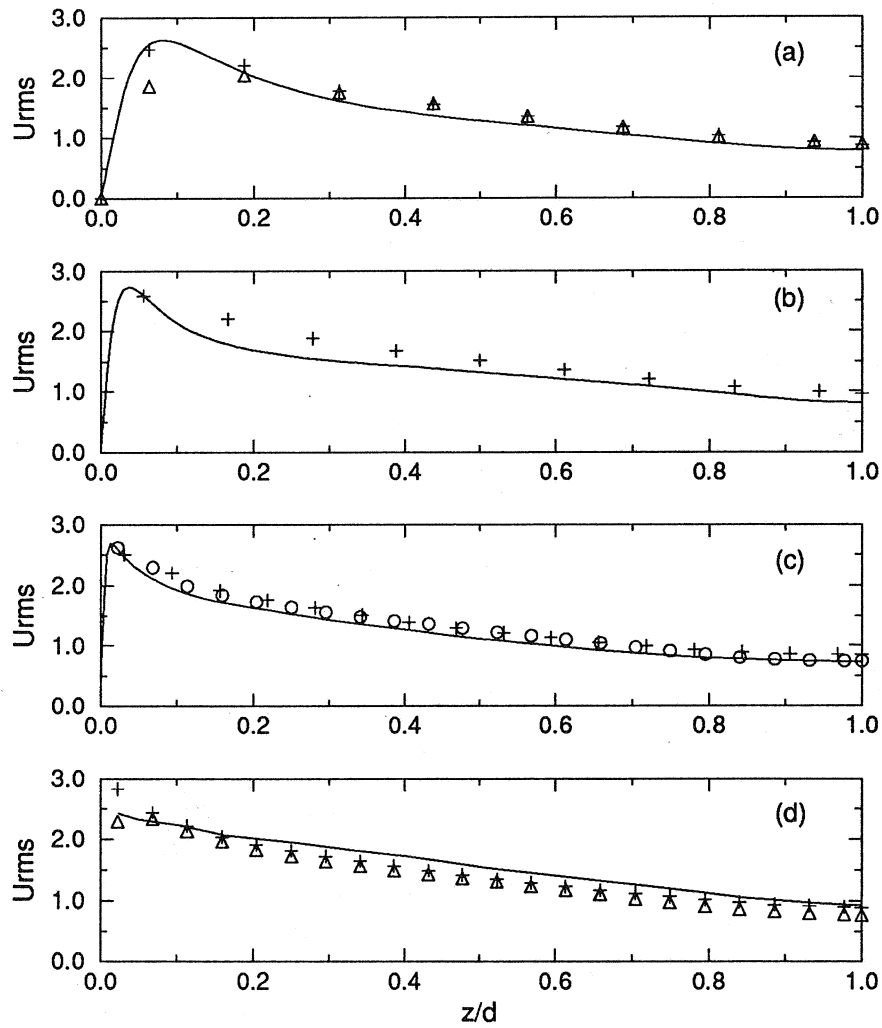


Figure 4.17: Streamwise turbulence intensities in outer coordinates (from Balaras *et al.* 1994). z is the wall-normal coordinate. (a) $Re_\tau = 200$, + dynamic model, Δ Smagorinsky model, — DNS (Kim *et al.* 1987); (b) $Re_\tau = 400$, + dynamic model, — DNS (Kim *et al.*, 1987); (c) $Re_\tau = 1,000$, + \circ dynamic model, — resolved LES (Piomelli 1993); (d) $Re_\tau = 5,000$, + dynamic model, Δ Smagorinsky model, — Experiment (Comte-Bellot 1963).

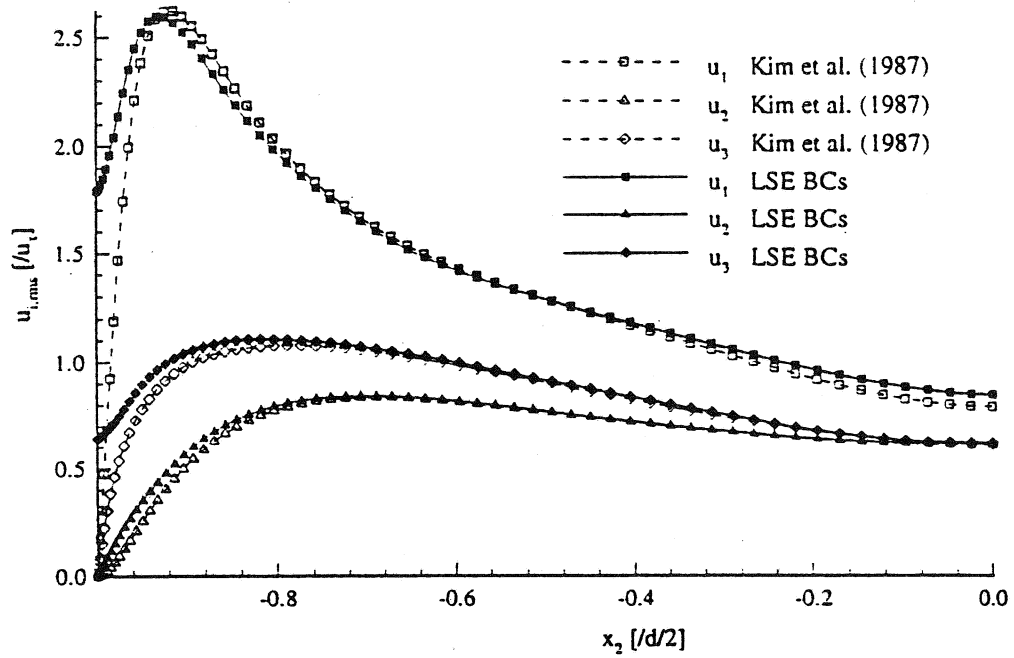


Figure 4.18: Turbulence intensities in outer coordinates (From Bagwell *et al.* 1993).

9. Backscatter modeling

One issue that has recently become a subject of attention is backscatter modeling. Most SGS models are absolutely dissipative; the actual SGS stresses, however, may transfer energy to the large scales (backscatter) at a given location, and while, on average, energy is transferred from large to small scales, reversed energy flow from small to large scales may also occur intermittently. Backscatter can also be significant in quasi-two-dimensional geophysical flows, in which an inverse energy cascade may exist. Most of the existing models are absolutely dissipative; only few of them, such as the mixed model and the dynamic model, are capable of predicting backscatter.

Piomelli *et al.* (1990a) showed that during the early nonlinear stages of transition energy is transferred from small to large scales even in the mean; failure to account for this phenomenon can cause inaccurate prediction of the growth of the perturbations. The Smagorinsky model predicted decay of the perturbations even in instances in which the flow should have been unstable. The findings of Piomelli *et al.* (1991) and Domaradzki *et al.* (1993, 1994) have already been discussed in Chapter 2. It should only be added here that Piomelli *et al.* (1991) found that backscatter depends on the type of filter used, being largest for the sharp Fourier cutoff, smallest for the Gaussian and intermediate for the top hat in real space. This finding indicates that perhaps backscatter modeling may be less critical in calculations that use finite-difference schemes than in those that use spectral methods.

Leith (1990), Chasnov (1991), and Mason and Thomson (1993), among others, have used models that include a stochastic backscatter force, that have given improved results over purely dissipative

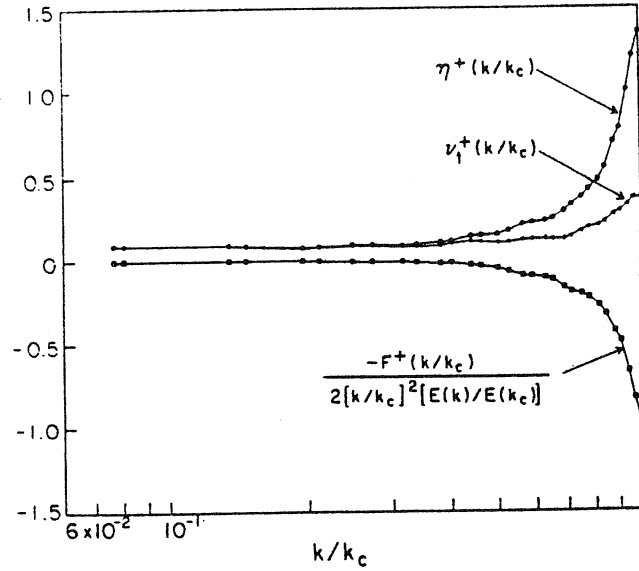


Figure 4.19: Subgrid-scale eddy viscosity, eddy-damping term and spectrum of the stochastic force computed from the LES of stationary turbulence (from Chasnov 1991).

models. Chasnov (1991) derived a stochastic backscatter force based on the EDQNM theory, and compared it with a standard eddy viscosity model in the LES of stationary turbulence. The backscatter force (Figure 4.19) resulted in better prediction of the inertial range of the spectrum.

Although stochastic backscatter forces have been successful when applied to unbounded flows,³ they could be less appropriate for the modeling of the near-wall region, where much of the momentum and energy transfer between subgrid and resolved scales is concentrated in coherent events whose locations appear to be correlated with large-scale turbulent structures, very much like Reynolds-stress production (Piomelli *et al.* 1991). The studies by Domaradzki *et al.* 1994, furthermore, indicate that the most important interaction between resolved and unresolved scales occurs between the scales belonging to the octaves above and below the cutoff. Under such conditions, a purely stochastic model of the energy transfer mechanisms would not be adequate, since it would decouple completely the subgrid scales from the large-scale events. A combination of a deterministic and a stochastic model may be required to represent the complex energy transfer mechanisms that take place near the wall of a boundary layer.

³The calculation by Mason and Thomson (1992) used approximate boundary conditions, and the near-wall region was not computed.

Chapter 5

Conclusions

In the hierarchy of methods for the solution of fluid flow problems, LES occupies an intermediate position between DNS and solution of the Reynolds-averaged Navier-Stokes equations (RANS). It will be successful as an engineering tool if its advantages over other techniques are exploited rather than if it is used to replace either DNS or RANS modeling.

The principal advantage of LES over DNS is the fact that it allows one to compute flows at Reynolds numbers much higher than those feasible in DNS, or at the same Reynolds numbers but at a considerably smaller expense. One should not expect to be able to extract from LES the same information as can be extracted from DNS, since modeling the small scales affects high-order statistics more than the lower-order ones. Thus, LES is expected to be more reliable for first and second moments, and to reproduce qualitatively the basic structures of the flows (existence of shear layers, vortical structures and so on).

Large-eddy simulation is considerably more expensive than RANS techniques for flows that are one- or two-dimensional in the mean and steady. For this reason, it should be applied to problems in which its cost is comparable to that of the solution of the RANS equations or to problems in which lower-level turbulence models fail. Such problems include unsteady or three-dimensional boundary layers, vortex-boundary layer interactions, separated flows and flows involving geometries with sharp corners (in square ducts, for example). Although in the near future LES will still be limited to fairly simple geometries, significantly more complex flows should be studied than those examined so far. Large eddy simulation of these flows can also be used to provide data for the development of more accurate lower-level models (especially pressure statistics, which are difficult to measure experimentally).

So far, several turbulent and transitional “building block” flows have been studied by LES: homogeneous turbulence, shear flows, channel flow and boundary layers. Two types of calculations have been performed: high Re , unbounded flows or wall-bounded flows with approximate boundary conditions, or low to moderate Re flows, with fairly good resolution. Well-resolved calculations yield velocity fields that can be used to obtain information on turbulence structure, and that can provide information for lower-level models (Bardina *et al.* 1983; Moin and Kim 1985; Kim and Moin 1986). Presently, three-dimensional or non-equilibrium flows are being studied (such as the backward-facing step, vortex/boundary layer interactions, or three-dimensional boundary layers).

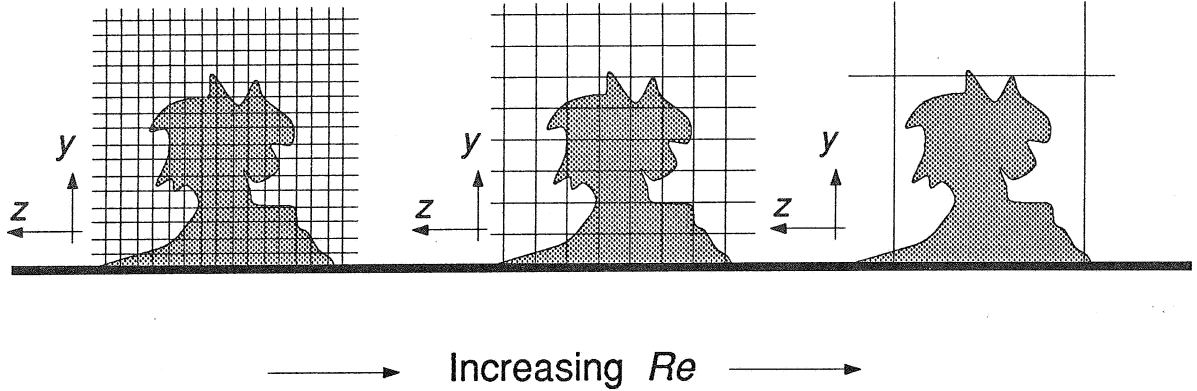


Figure 5.1: Grid resolution and near-wall structures.

Large-eddy simulation research in engineering continues in many areas, with a particular focus on the following: the continued effort to devise more accurate models, especially for the near-wall region, the application to “complex flows”, and, finally, the application of LES to compressible and reacting flows. The first issue is particularly important, in the writer’s opinion, because of the need to extend LES to high Reynolds number flows, in which resolution of even the large structures in the near-wall region becomes unaffordable. If one considers a turbulent event occurring near a solid boundary (the shaded area in Figure 5.1); the energy produced by this event, if the mesh is very fine, appears in the equation for the average large-scale energy $\langle \overline{u_i'' u_i''} \rangle$, equation (2.21) through the term $-2 \langle \overline{u_i'' u_j''} \rangle \frac{\partial U_i}{\partial x_j}$ (term C). If the grid is coarsened or, equivalently, the Reynolds number increased for a constant mesh spacing, part of the event becomes due to the unresolved scales, and the energy produced by it must be accounted partly by term C, partly by the SGS production (term D) $-2 \langle \tau_{ij} \rangle \frac{\partial U_i}{\partial x_j}$. If the mesh is coarsened further (or the Reynolds number increased), all of the energy production occurs at the subgrid-scale level, and must be taken into account either through approximate boundary conditions, or through modifications to the eddy viscosity.

The application of LES to non-equilibrium flows is a subject of great technological importance. For the time being, although the geometry constraints are being gradually removed as finite difference schemes supplant the spectral methods widely in use until now, the application of LES to engineering calculations in very complex geometries is not yet feasible. It may be perhaps more beneficial instead to use LES for detailed studies of the turbulence physics at moderate Reynolds numbers in non-canonical flows, to understand the basic phenomena at play in new flow configurations, and to provide data for RANS models. Typical problems that are within the present capabilities of LES are flows that are three-dimensional in the mean, in fairly simple geometries, but that include one or more phenomena (extra strains, separation, pressure gradients, for example) that occur in more complex engineering flows.

Although the first applications of LES to compressible and reacting flows were relatively recent, much progress has already been made in this area. All of the most popular models have been extended to compressible flows, and a number of test cases have been examined. While many of the concerns that apply to incompressible applications (model accuracy, backscatter and so on)

extend also to compressible flows, additional difficulties are due to the fact that the equations are more complex and shock wave interactions and eddy shocklets may occur; furthermore, finite differences introduce artificial dissipation, the effect of which must be studied and compared with that of the SGS dissipation. Aliasing errors can also be more significant, owing to the presence of triple products in the equations of motion. The simulation and modeling of flows including chemical reactions is still in its infancy.

Although large eddy simulations in engineering have not enjoyed a rapid development similar to that of direct simulations, the renewed activity in LES justifies an optimistic view of the future of this technique. One would hope that, ten years from today, LES of engineering problems will be routinely performed on a desktop workstation. To achieve this end a continued effort is required by the research community, involving increased interactions among its members. Experiments, direct simulations and numerical analysis are all necessary for further progress. The interaction between geophysical scientists and engineers, which has not been particularly noteworthy so far, must be enhanced to facilitate the development of LES into a practical tool useful in both fields.

Chapter 6

Bibliography

- AUPOIX, B. (1985) In *Finite Approx. in Fluid Mech.*, edited by E.H. Hirschel (Vieweg, Braunschweig), 37.
- BAGWELL, T.G., ADRIAN, R.J., KIM, J., AND MOSER, R.D. (1993) In *Near-Wall Turbulent Flows*, edited by R.M.C. So, C.G. Speziale and B.E. Launder, (Elsevier, Amsterdam), 265.
- BAGWELL, T.G. (1994) *Ph.D. Dissertation, Univ. of Ill. at Urbana Champaign*.
- BALARAS, E., BENOCCHI, C., AND PIOMELLI, U. (1994) In press, *Theoret. Comput. Fluid Dyn.*
- BALINT, J.-L., WALLACE, J.M., AND VUKOSLAVČEVIĆ, P. (1991) *J. Fluid Mech.* **228**, 53.
- BARDINA, J., FERZIGER, J.H., AND REYNOLDS, W.C. (1980) *AIAA Paper No. 80-1357*.
- BARDINA, J., FERZIGER, J.H., AND REYNOLDS, W.C. (1983) *Department of Mechanical Engineering Report TF-19*, Stanford, California.
- BARDINA, J., FERZIGER, J.H., AND ROGALLO, R.S. (1985) *J. Fluid Mech.* **154**, 321.
- CAMBON, C., JEANDEL, D., AND MATHIEU, J. (1981) *J. Fluid Mech.* **104**, 247.
- CHASNOV, J.R. (1991) *Phys. Fluids A* **3**, 188.
- CHOLLET, J.-P. AND LESIEUR, M. (1981) *J. Atmos. Sci.* **38**, 2747.
- CHOLLET, J.-P. (1985) In *Turbulent shear flows 4*, edited by L.J.S. Bradbury, F. Durst, B.E. Launder, F.W. Schmidt, and J.H. Whitelaw (Springer-Verlag, Berlin), 62.
- CLARK, R.A., FERZIGER, J.H., AND REYNOLDS, W.C. (1979) *J. Fluid Mech.* **91**, 1.
- COMTE-BELLOT, G. (1963) *Ph.D. Thesis, University of Grenoble*.
- DANG, K.T. (1985) *AIAA J.* **23**, 221.
- DANG, K.T. AND DESCHAMPS, V. (1987) In *Numerical Methods in Laminar and Turbulent Flows*, edited by C. Taylor, W.G. Habashi, and M.M. Hafez (Pine Ridge, Swansea), 423.
- DEARDORFF, J.W. (1970) *J. Fluid Mech.* **41**, 453.
- DOMARADZKI, J.A., LIU, W., AND BRACHET, M.E. (1993) *Phys. Fluids A* **5**, 1747.
- DOMARADZKI, J.A., LIU, W., HÄRTEL, C., AND KLEISER, L. (1994) *Phys. Fluids* **6**, 1583.
- ESMAILI, H. AND PIOMELLI, U. (1993) In *Near-Wall Turbulent Flows*, edited by R.M.C. So, C.G. Speziale and B.E. Launder, (Elsevier, Amsterdam), 287.
- FAVRE, A. (1965a) *J. de Mécanique* **4**, 361.
- FAVRE, A. (1965b) *J. de Mécanique* **4**, 391.

- GERMANO, M. (1986) *Phys. Fluids* **29**, 2323.
- GERMANO, M., PIOMELLI, U., MOIN, P., AND CABOT, W.H. (1991) *Phys. Fluids A* **3**, 1760.
- GERMANO, M. (1992) *J. Fluid Mech.* **238**, 235.
- GHOSAL, S., LUND, T. AND MOIN, P. (1993) In *Annual Research Briefs - 1993*, (Center for Turbulence Research, Stanford University), 1.
- GHOSAL, S. (1994) In *Annual Research Briefs - 1993*, (Center for Turbulence Research, Stanford University), 111.
- GRÖTZBACH, G. (1981) *Int. J. Heat Mass Transfer* **24**, 475.
- HORIUTI, K. AND YOSHIZAWA, A. (1985) In *Finite Approx. in Fluid Mech.*, edited by E.H. Hirschel (Vieweg, Braunschweig), 119.
- HORIUTI, K. (1987) *J. Comput. Phys.* **71**, 343.
- HORIUTI, K. (1989) *Phys. Fluids A* **1**, 426.
- HUSSAIN, A.K.M.F., AND REYNOLDS, W.C. (1975) *J. Fluids Engng* **97**, 568.
- KIM, J. AND MOIN, P. (1986) *J. Fluid Mech.* **162**, 339.
- KIM, J., MOIN, P., AND MOSER, R.D. (1987) *J. Fluid Mech.* **177**, 133.
- KRAICHNAN, R.H. (1976) *J. Atmos. Sci.* **33**, 1521.
- LAUFER, J. (1951) *NACA Report 1053*.
- LEITH, C.E. (1990) *Phys. Fluids A* **2**, 297.
- LEONARD, A. (1974) *Adv. Geophys.* **18A**, 237.
- LESIEUR, M. (1990) *Turbulence in fluids* (Kluwer, Dordrecht).
- LILLY, D.K. (1966) *NCAR Manuscript No. 123*, Boulder, Colorado.
- LILLY, D.K. (1967) In *Proc. IBM Sci. Comp. Symp. on Environmental Sciences*, Yorktown Heights, NY.
- LILLY, D.K. (1992) *Phys. Fluids A* **4**, 633.
- LUND, T. (1990) In *Instability and Transition*, edited by M.Y. Hussaini and R.G. Voigt (Springer-Verlag, New York), **2**, 463.
- MADABUSHI, R.K. AND VANKA, P. (1991) *Phys. Fluids A* **3**, 2734.
- MASON, P.J. AND CALLEN, N.S. (1986) *J. Fluid Mech.* **162**, 439.
- MASON, P.J. AND THOMSON, D.J. (1992) *J. Fluid Mech.* **242**, 51.
- MCMILLAN, O.J., FERZIGER, J.H., AND ROGALLO, R.S. (1980) *AIAA Paper No. 80-1339*.
- MÉTAIS, O. AND LESIEUR, M. (1992) *J. Fluid Mech.* **239**, 157.
- MOIN, P., REYNOLDS, W.C., AND FERZIGER, J.H. (1978) *Department of Mechanical Engineering Report TF-12*, Stanford, California.
- MOIN, P. AND KIM, J. (1982) *J. Fluid Mech.* **118**, 341.
- MOIN, P. AND KIM, J. (1985) *J. Fluid Mech.* **155**, 441.
- MOIN, P., SQUIRES, K., CABOT, W.H., AND LEE, S. (1991) *Phys. Fluids A* **3**, 2746.
- MOSER, R.D. AND MOIN, P. (1987) *J. Fluid Mech.* **175**, 479.
- NAGUIB, A.M. AND WARK, C.E. (1992) *J. Fluid Mech.* **243**, 541.

- NORMAND, X. AND LESIEUR, M. (1992) *Theor. Comput. Fluid Dynamics* **3**, 231.
- PIOMELLI, U., MOIN, P., AND FERZIGER, J.H. (1988) *Phys. Fluids* **31**, 1984.
- PIOMELLI, U., ZANG, T.A., SPEZIALE, C.G., AND HUSSAINI, M.Y. (1990a) *Phys. Fluids A* **2**, 257.
- PIOMELLI, U., ZANG, T.A., SPEZIALE, C.G., AND LUND, T.S. (1990b) In *Instability and Transition*, edited by M.Y. Hussaini and R.G. Voigt (Springer-Verlag, New York), **2**, 480.
- PIOMELLI, U., CABOT, W.H., MOIN, P., AND LEE, S. (1991a) *Phys. Fluids A* **3**, 1766.
- PIOMELLI, U. AND ZANG, T.A. (1991b) *Computer Phys. Comm.* **65**, 224.
- PIOMELLI, U. (1993) *Phys. Fluids A* **5**, 1484.
- REYNOLDS, W.C. (1990) In *Whither turbulence? Turbulence at the crossroads*, edited by J.L. Lumley (Springer-Verlag, Heidelberg), 313.
- RICHTER, J.P. (1970) *The notebooks of Leonardo da Vinci* (Dover, New York).
- ROGALLO, R.S. AND MOIN, P. (1984) *Ann. Rev. Fluid Mech.* **16**, 99.
- SCHUMANN, U. (1975) *J. Comput. Phys.* **18**, 376.
- SMAGORINSKY, J. (1963) *Monthly Weather Review* **91**, 99.
- SMITH, L.M. AND YAKHOT, V. (1993) *Theoret. Comput. Fluid Dyn.* **4**, 197.
- SPALART, P.R. AND WATMUFF, J.H. (1993) *J. Fluid Mech.* **249**, 337.
- SPEZIALE, C.G. (1985) *J. Fluid Mech.* **156**, 55.
- SPEZIALE, C.G., ERLEBACHER, G., ZANG, T.A., AND HUSSAINI, M.Y. (1988) *Phys. Fluids A* **31**, 940.
- SQUIRES, K.D. AND PIOMELLI, U. (1994) In press, *Turbulent Shear Flows 9*, edited by F. Durst, N. Kasagi, B.E. Launder, F.W. Schmidt and J.H. Whitelaw, (Springer Verlag, Heidelberg).
- STREET AND MACARAEG (1989) *Int. J. Applied Num. Math.* **6**, 123
- TAFTI, D. AND VANKA, P. (1992) *Phys. Fluids A* **3**, 642.
- VAN DRIEST, E.R. (1956) *J. Aerospace Sci.* **23**, 1007.
- WEI, T. AND WILLMARTH, W.W. (1989) *J. Fluid Mech.* **204**, 57.
- YAKHOT, A., ORSZAG, S.A., YAKHOT, V., AND ISRAELI, M. (1989) *J. Sci. Computing* **4**, 139.
- YAKHOT, V. AND ORSZAG, S.A. (1986) *J. Sci. Computing* **1**, 3.
- YOSHIZAWA, A. (1982) *Phys. Fluids* **25**, 1532.
- YOSHIZAWA, A. (1987) In *Encyclopedia of Fluid Mechanics*, edited by N.P. Cheremisinoff (Gulf Publishing, West Orange), **6**, 1277.
- ZANG, T.A., GILBERT, N., AND KLEISER, L. (1990) In *Instability and Transition*, edited by M.Y. Hussaini and R.G. Voigt (Springer-Verlag, New York), **1**, 283.
- ZANG, T.A., DAHLBURG, R.B., AND DAHLBURG, J.P. (1992) *Phys. Fluids A* **4**, 127.
- ZANG, T.A., AND PIOMELLI, U. (1993) In *Large Eddy Simulation of Complex Engineering and Geophysical Flows*, edited by B. Galperin and S.A. Orszag, (Cambridge University Press, Cambridge), 209.
- ZANG, Y., STREET, R.L., AND KOSEFF, J. (1993a) In *Annual Research Briefs - 1992*, (Center for Turbulence Research, Stanford), 85.
- ZANG, Y., STREET, R.L., AND KOSEFF, J. (1993b) *Phys. Fluids A* **5**, 3186.

List of Recent TAM Reports

No.	Authors	Title	Date
716	Sofronis, P.	Linearized hydrogen elasticity	July 1993
717	Nitzsche, V. R., and K. J. Hsia	Modelling of dislocation mobility controlled brittle-to-ductile transition	July 1993
718	Hsia, K. J., and A. S. Argon	Experimental study of the mechanisms of brittle-to-ductile transition of cleavage fracture in silicon single crystals	July 1993
719	Cherukuri, H. P., and T. G. Shawki	An energy-based localization theory: Part II—Effects of the diffusion, inertia and dissipation numbers	Aug. 1993
720	Aref, H., and S. W. Jones	Chaotic motion of a solid through ideal fluid	Aug. 1993
721	Stewart, D. S.	Lectures on detonation physics: Introduction to the theory of detonation shock dynamics	Aug. 1993
722	Lawrence, C. J., and R. Mei	Long-time behavior of the drag on a body in impulsive motion	Sept. 1993
723	Mei, R., J. F. Klausner, and C. J. Lawrence	A note on the history force on a spherical bubble at finite Reynolds number	Sept. 1993
724	Qi, Q., R. E. Johnson, and J. G. Harris	A re-examination of the boundary layer attenuation and acoustic streaming accompanying plane wave propagation in a circular tube	Sept. 1993
725	Turner, J. A., and R. L. Weaver	Radiative transfer of ultrasound	Sept. 1993
726	Yogeswaren, E. K., and J. G. Harris	A model of a confocal ultrasonic inspection system for interfaces	Sept. 1993
727	Yao, J., and D. S. Stewart	On the normal detonation shock velocity-curvature relationship for materials with large activation energy	Sept. 1993
728	Qi, Q.	Attenuated leaky Rayleigh waves	Oct. 1993
729	Sofronis, P., and H. K. Birnbaum	Mechanics of hydrogen-dislocation-impurity interactions: Part I—Increasing shear modulus	Oct. 1993
730	Hsia, K. J., Z. Suo, and W. Yang	Cleavage due to dislocation confinement in layered materials	Oct. 1993
731	Acharya, A., and T. G. Shawki	A second-deformation-gradient theory of plasticity	Oct. 1993
732	Michaleris, P., D. A. Tortorelli, and C. A. Vidal	Tangent operators and design sensitivity formulations for transient nonlinear coupled problems with applications to elasto-plasticity	Nov. 1993
733	Michaleris, P., D. A. Tortorelli, and C. A. Vidal	Analysis and optimization of weakly coupled thermo-elasto-plastic systems with applications to weldment design	Nov. 1993
734	Ford, D. K., and D. S. Stewart	Probabilistic modeling of propellant beds exposed to strong stimulus	Nov. 1993
735	Mei, R., R. J. Adrian, and T. J. Hanratty	Particle dispersion in isotropic turbulence under the influence of non-Stokesian drag and gravitational settling	Nov. 1993
736	Dey, N., D. F. Socie, and K. J. Hsia	Static and cyclic fatigue failure at high temperature in ceramics containing grain boundary viscous phase: Part I—Experiments	Nov. 1993
737	Dey, N., D. F. Socie, and K. J. Hsia	Static and cyclic fatigue failure at high temperature in ceramics containing grain boundary viscous phase: Part II—Modelling	Nov. 1993
738	Turner, J. A., and R. L. Weaver	Radiative transfer and multiple scattering of diffuse ultrasound in polycrystalline media	Nov. 1993
739	Qi, Q., and R. E. Johnson	Resin flows through a porous fiber collection in pultrusion processing	Dec. 1993
740	Weaver, R. L., W. Sachse, and K. Y. Kim	Transient elastic waves in a transversely isotropic plate	Dec. 1993
741	Zhang, Y., and R. L. Weaver	Scattering from a thin random fluid layer	Dec. 1993

(continued on next page)

List of Recent TAM Reports (cont'd)

<i>No.</i>	<i>Authors</i>	<i>Title</i>	<i>Date</i>
742	Weaver, R. L., and W. Sachse	Diffusion of ultrasound in a glass bead slurry	Dec. 1993
743	Sundermeyer, J. N., and R. L. Weaver	On crack identification and characterization in a beam by nonlinear vibration analysis	Dec. 1993
744	Li, L., and N. R. Sottos	Predictions of static displacements in 1-3 piezocomposites	Dec. 1993
745	Jones, S. W.	Chaotic advection and dispersion	Jan. 1994
746	Stewart, D. S., and J. Yao	Critical detonation shock curvature and failure dynamics: Developments in the theory of detonation shock dynamics	Feb. 1994
747	Mei, R., and R. J. Adrian	Effect of Reynolds-number-dependent turbulence structure on the dispersion of fluid and particles	Feb. 1994
748	Liu, Z.-C., R. J. Adrian, and T. J. Hanratty	Reynolds-number similarity of orthogonal decomposition of the outer layer of turbulent wall flow	Feb. 1994
749	Barnhart, D. H., R. J. Adrian, and G. C. Papen	Phase-conjugate holographic system for high-resolution particle image velocimetry	Feb. 1994
750	Qi, Q., W. D. O'Brien Jr., and J. G. Harris	The propagation of ultrasonic waves through a bubbly liquid into tissue: A linear analysis	Mar. 1994
751	Mittal, R., and S. Balachandar	Direct numerical simulation of flow past elliptic cylinders	May 1994
752	Anderson, D. N., J. R. Dahlen, M. J. Danyluk, A. M. Dreyer, K. M. Durkin, J. J. Kriegsmann, J. T. McGonigle, and V. Tyagi	Thirty-first student symposium on engineering mechanics, J. W. Phillips, coord.	May 1994
753	Thoroddsen, S. T.	The failure of the Kolmogorov refined similarity hypothesis in fluid turbulence	May 1994
754	Turner, J. A., and R. L. Weaver	Time dependence of multiply scattered diffuse ultrasound in polycrystalline media	June 1994
755	Riahi, D. N.	Finite-amplitude thermal convection with spatially modulated boundary temperatures	June 1994
756	Riahi, D. N.	Renormalization group analysis for stratified turbulence	June 1994
757	Riahi, D. N.	Wave-packet convection in a porous layer with boundary imperfections	June 1994
758	Jog, C. S., and R. B. Haber	Stability of finite element models for distributed-parameter optimization and topology design	July 1994
759	Qi, Q., and G. J. Brereton	Mechanisms of removal of micron-sized particles by high-frequency ultrasonic waves	July 1994
760	Shawki, T. G.	On shear flow localization with traction-controlled boundaries	July 1994
761	Balachandar, S., D. A. Yuen, and D. M. Reuteler	High Rayleigh number convection at infinite Prandtl number with temperature-dependent viscosity	July 1994
762	Phillips, J. W.	Arthur Newell Talbot—Proceedings of a conference to honor TAM's first department head and his family	Aug. 1994
763	Man., C. S., and D. E. Carlson	On the traction problem of dead loading in linear elasticity with initial stress	Aug. 1994
764	Zhang, Y., and R. L. Weaver	Leaky Rayleigh wave scattering from elastic media with random microstructures	Aug. 1994
765	Cortese, T. A., and S. Balachandar	High-performance spectral simulation of turbulent flows in massively parallel machines with distributed memory	Aug. 1994
766	Balachandar, S.	Signature of the transition zone in the tomographic results extracted through the eigenfunctions of the two-point correlation	Sept. 1994
767	Piomelli, U.	Large-eddy simulation of turbulent flows	Sept. 1994